(Theos *et al.*, 2005). In subsequent stages of maturation, melanosomes undergoing eumelanogenesis always exhibit an ellipsoidal shape and form regular parallel intralumenal fibers (Stage II). Melanins are deposited on these fibrillae, resulting in a progressively pigmented internal matrix (Stage III). Melanin synthesis and deposition continue until little or no internal structure becomes visible (Stage IV). However, the precise mechanism of melanosome biogenesis is still unclear.

To clarify the molecular mechanism of melanosome biogenesis in more detail, we analyzed the functional relationship between Rab7 and gp100. Interestingly, we found that Rab7 was colocalized with gp100 in Stage I melanosomes. Moreover, our studies revealed that Rab7 may play an important role in promoting the gp100 maturation.

RESULTS

Rab7 is colocalized with full-length gp100 in Stage I melanosomes

To explore the functional relationship between Rab7 and gp100, we first examined, using a confocal microscope, the subcellular localization of Rab7 and the endogenous, full-length gp100, which is distributed in Stage I melanosomes and is recognized by the anti-gp100 antibody, αPEP13h (Yasumoto *et al.*, 2004). In addition to the full-length gp100, however, αPEP13h is able to recognize the C-terminal fragments (~27-kDa) of gp100 generated by proteolysis as well (Figure 3a). However, the C-terminal fragments are not carried over to Stage II and later-stage melanosomes, because the fragments are unstable and rapidly degraded before the stage of melanosome shifts from I to II (Berson *et al.*, 2003; Yasumoto *et al.*, 2004). Therefore, this antibody detects solely gp100 (full-length gp100 and its C-terminal fragments) that is present in Stage I melanosomes in melanoma cells.

MMAc cells were transiently transfected with pEYFP empty vector, pEYFP-Rab7-wild-type (WT), pEYFP-Rab7-Q67L (a GTPase-deficient, dominant-active mutant), or pEYFP-Rab7-T22N (a GDP-bound, dominant-negative mutant). We found that yellow fluorescent proteins (YFP)-Rab7-WT and YFP-Rab7-Q67L were visualized as punctuated structures and considerably colocalized with the endogenous full-length gp100 in the perinuclear region (Figure 1). When endogenous Rab7 was detected using indirect immunofluorescence, essentially the same result was obtained (data not shown). In contrast, YFP-Rab7-T22N exhibited a diffuse intracellular localization pattern and failed to colocalize with the full-length protein. Similar results were obtained with endogenous MART-1, which was reported to interact and colocalize with gp100 in melanoma cells (De Maziere *et al.*, 2002; Hoashi *et al.*, 2005), thus confirming that this gp100-interacting protein was partly colocalized with YFP-Rab7-WT and YFP-Rab7-Q67L, but not with YFP-Rab7-T22N in MMAc cells (data not shown).

To substantiate the melanosomal distribution of Rab7, we investigated whether Rab7-WT and Rab7-Q67L were colocalized with lysosomal-associated membrane protein 2 (LAMP-2), which is colocalized with the full-length gp100-stained with αPEP13h in the perinuclear region in melanocytes and SK-MEL-28 melanoma cells (Hoashi *et al.*, 2005). We also confirmed the colocalization between LAMP-2 and

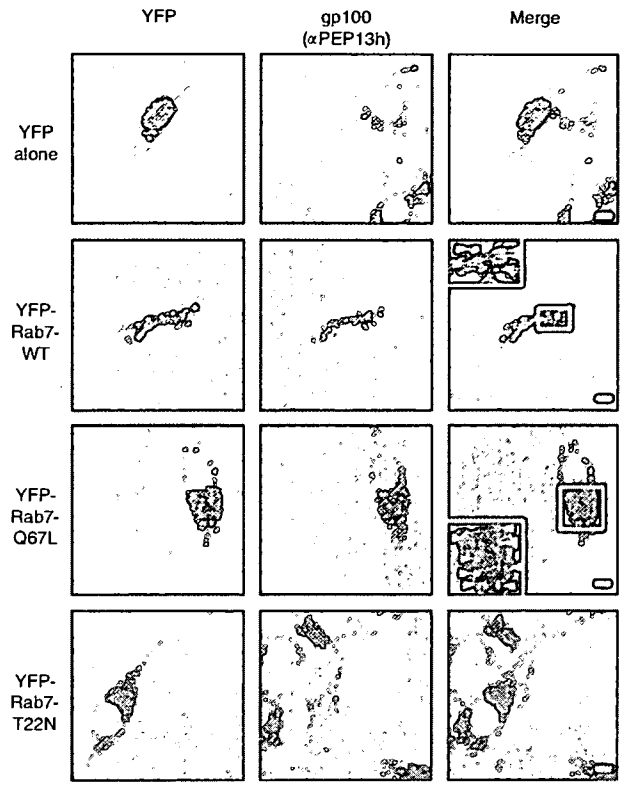

Figure 1. Rab7-WT and Rab7-Q67L are colocalized with full-length, immature gp100 in the perinuclear region. MMAc cells were transfected with pEYFP empty vector, pEYFP-Rab7-WT, pEYFP-Rab7-Q67L, or pEYFP-Rab7-T22N. After 2 days, the cells were fixed and immunostained with αPEP13h and Alexa Fluor 594-conjugated secondary antibody. Bars, 10 μm. Insets, × 2 magnification of the indicated regions. Structures colocalized for full-length gp100 and either Rab7-WT or Rab7-Q67L are indicated by arrowheads.

αPEP13h-recognized gp100 in the perinuclear region in MMAc cells (data not shown). As shown in Figure 2, YFP-Rab7-WT and YFP-Rab7-Q67L, but not YFP-Rab7-T22N, were colocalized exclusively with this marker protein (LAMP-2) in the perinuclear region of MMAc melanoma cells. On the other hand, the *cis*-Golgi marker GM130 and the endoplasmic reticulum marker KDEL failed to exhibit any colocalization (data not shown). Taken together, these results suggest that the GTP-bound form of the Rab7 protein is, at least in part, distributed to Stage I melanosomes, with which the full-length gp100 is associated in MMAc melanoma cells.

To validate that the GTP-bound form of Rab7 is associated with Stage I, but not Stage II–IV, melanosomes, MMAc cells were stained with another anti-gp100 antibody HMB45, which recognizes only the processed, mature gp100 (Hoashi *et al.*, 2006) (Figure 3a). Interestingly, neither YFP-Rab7-WT nor YFP-Rab7-Q67L was colocalized with the mature gp100 (Figure 3b), further supporting the localization of Rab7-WT and Rab7-Q67L to Stage I, but not Stage II–IV, melanosomes. These results collectively suggest that the GTP-bound form of Rab7 protein is, at least in part, colocalized with the full-length gp100 in Stage I melanosomes.

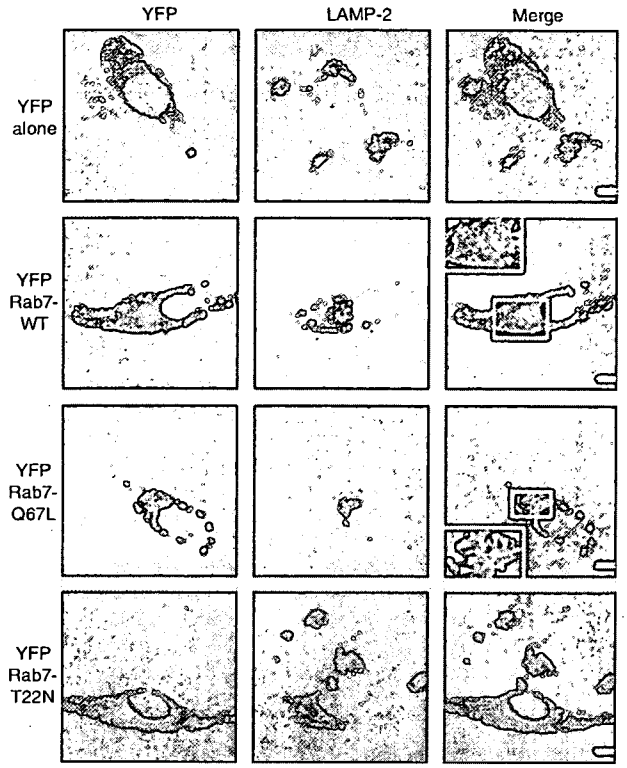

Figure 2. Rab7-WT and Rab7-Q67L are colocalized with LAMP-2 in the perinuclear region. MMAc cells were transfected with pEYFP empty vector, pEYFP-Rab7-WT, pEYFP-Rab7-Q67L, or pEYFP-Rab7-T22N. After 2 days, the cells were fixed and immunostained with anti-LAMP-2 antibody and Alexa Fluor 594-conjugated secondary antibody. Bars, 10 μm. Insets, ×2 magnification of the indicated regions. Structures colocalized for LAMP-2 and either Rab7-WT or Rab7-Q67L are indicated by arrowheads.

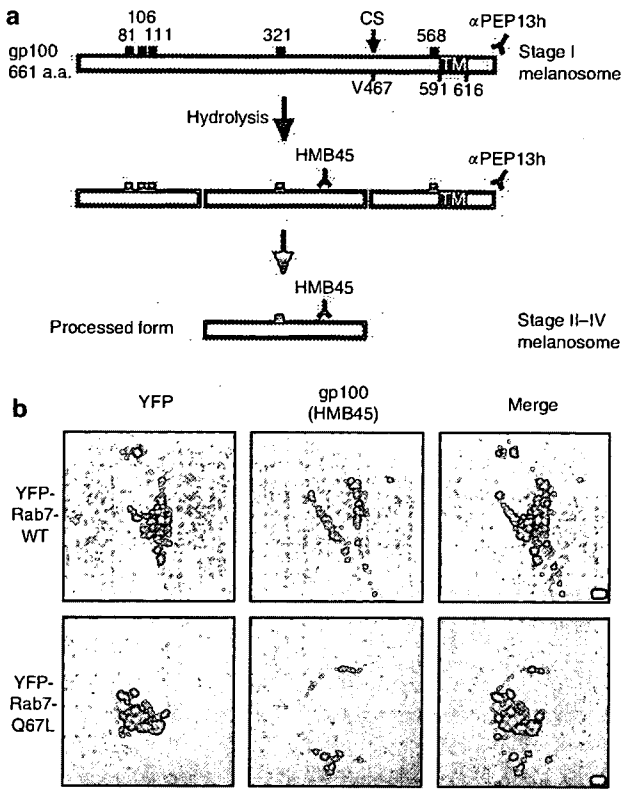

Figure 3. Rab7-WT and Rab7-Q67L fail to be colocalized with processed, mature gp100. (a) Schematic presentation of the processing and epitope mapping of gp100 (Yasumoto *et al.*, 2004). gp100 is shown as the complete native protein at the top of the figure and in its processed/matured forms in the middle and bottom of the figure. Potential N-glycosylation sites at 81, 106, 111, 321, and 568 are indicated. Val-467 (V467) refers to the potential cleavage site (CS) during maturation of Stage I to Stage II melanosomes. TM, transmembrane domain; inverted Ys, antibodies. (b) MMAc cells were transfected with either pEYFP-Rab7-WT or pEYFP-Rab7-Q67L. After 2 days, the cells were fixed and immunostained with HMB45 and Alexa Fluor 594-conjugated secondary antibody. Bar = 10 μm.

Rab7 and its dominant-active mutant (Rab7-Q67L) promote the maturation of gp100

It is known that the cleavage events of gp100, as a part of its maturation process, occur in Stage I melanosomes (Yasumoto *et al.*, 2004). Thus, the finding that Rab7-WT and Rab7-Q67L were colocalized with the immature gp100 in Stage I melanosomes led us to investigate whether Rab7 activity plays a pivotal role in the regulation of the proteolytic cleavage of gp100. To quantify mature gp100, we carried out Western blot analysis of lysates from MMAc cells expressing Rab7-WT and its mutants, using the anti-gp100 antibody HMB45, which recognizes only the cleaved, mature forms of gp100. It was confirmed that the mature gp100 was detected as several bands in the 30-kDa range, including 32- and 29-kDa bands (Figure 4a, top panel), which are due to proteolytic cleavage at multiple sites during the maturation (Yasumoto *et al.*, 2004; Hoashi *et al.*, 2006). Interestingly, we found that overexpression of the dominant-active mutant (Rab7-Q67L) and, to a lesser extent, Rab7-WT significantly increased the protein levels of the processed, mature forms of gp100 (32- and 29-kDa bands) (Figure 4a, top panel and b). However, although the dominant-negative mutant (Rab7-T22N) was expressed at almost the same extent—or even higher—compared with the WT protein and the dominant-active mutant, respectively (Figure 4a, lower middle panel), the mutant did not show such an effect. Rab7-T22N, if anything, slightly decreased the protein levels of the mature forms of gp100 (Figure 4b). On the other hand, the amounts of full-length gp100 (100-kDa band) were not markedly changed by the expression of Rab7-WT and Rab7-Q67L (Figure 4a, upper middle panel and c). These results suggest that Rab7 increased the amounts of mature gp100 by enhancing its post-translational modification (proteolytic cleavage) but not transcription/translation.

As shown in Figure 4b, the dominant-negative mutant (Rab7-T22N) only slightly decreased the protein levels of the mature forms of gp100. We speculated that the relatively low effectiveness was probably caused by the low transfection efficiencies (around 40%) of Rab7 cDNA constructs to MMAc cells. It should also be noted that endogenous Rab7 is highly expressed (when detected by anti-Rab7 antibody, signal intensities of the over-expressed Rab7 bands were at most

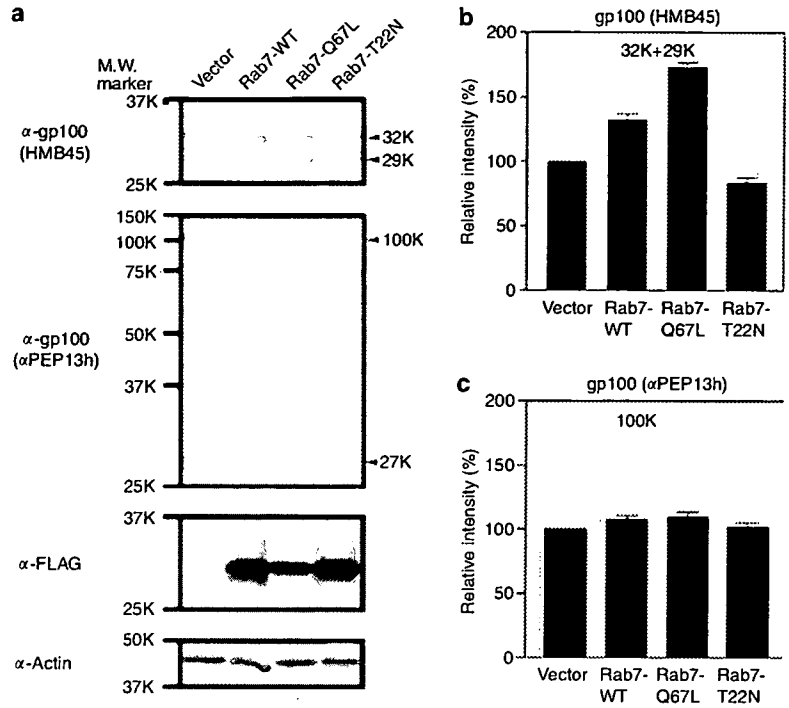

Figure 4. Overexpression of Rab7-WT and Rab7-Q67L promotes the maturation of gp100. (a) MMAc cells were transfected with p3xFLAG-CMV empty vector, p3xFLAG-CMV-Rab7-WT, p3xFLAG-CMV-Rab7-Q67L, or p3xFLAG-CMV-Rab7-T22N. After 2 days, the cells were harvested and analyzed by Western blotting using anti-FLAG M2 antibody, αPEP13h, HMB45, or anti-actin antibody, as indicated. Equal amounts of protein were loaded in each lane. (**b** and **c**) The band intensities of mature gp100 (32- + 29-kDa bands detected by HMB45) (**b**) and full-length gp100 (100-kDa band detected by αPEP13h) (**c**) were quantified and then normalized for those of actin. The results represent the mean ± SEM of the values obtained in five separate experiments. The value of p3xFLAG-CMV vector-transfected cells was set at 100.

only two-fold higher than those of endogenous Rab7) (data not shown). Thus, to circumvent the problem of the low transfection efficiency, we performed small interfering RNA (siRNA) experiments because the transfection efficiency of short RNA (siRNA) is much higher (>80%) than that of long DNA (Rab7 cDNA constructs). Indeed, siRNA that specifically targets Rab7 (Jager *et al.*, 2004) successfully and significantly reduced Rab7 protein expression 76.7±6.3% (mean±S.E., $n=4$) in MMAc cells (Figure 5a, top panel), as reported by Jager *et al.* (Jager *et al.*, 2004). In marked contrast to the over-expression experiments (Figure 4a, top panel and b), the Rab7 siRNA significantly reduced the protein levels of mature gp100 (32- and 29-kDa bands) compared with the control siRNA (Figure 5a, upper middle panel and b). It is expected that the levels of the 100-kDa band should increase if the processing is disrupted. Indeed, the amount of full-length gp100 (100-kDa band) was slightly but clearly augmented by the Rab7 knockdown (Figure 5a, lower middle panel and c). It is also possible that the siRNA knockdown of Rab7 leads to mistargeting rather than defects in processing (proteolysis). However, abnormal localization of gp100 was not observed in MMAc cells transfected with Rab7 siRNA (data not shown). Taken together, these results further support that Rab7 enhances the maturation of gp100 by promoting the proteolytic cleavage of gp100 in Stage I melanosomes.

DISCUSSION

Melanosome biogenesis consists of complex multistep processes that involve protein synthesis, vesicle transport/fusion, and post-translational modifications such as glycosylation, proteolysis, and oligomerization. Moreover, these processes are regulated in a complicated manner. Because of the complexity, the detailed molecular mechanism of melanosome biogenesis is still elusive. In particular, gp100 is one of the most enigmatic proteins involved in the melanogenesis. This study shows that Rab7 plays an important role in promoting gp100 maturation. Thus, Rab7 positively regulates the process of melanosome biogenesis via not only transport of TYRP-1 and tyrosinase (Gomez *et al.*, 2001; Hirosaki *et al.*, 2002) but also maturation of gp100. Melanins are deposited on the fibrillar matrix formed by the mature gp100, resulting in a progressively pigmented internal matrix (Theos *et al.*, 2005). Thus, a disruption of the gp100 maturation caused by the Rab7 dysfunction would lead to a delay and/or reduction of the pigmentation. However, further studies are required to elucidate how the reduced amount of mature gp100 generally affects melanogenesis.

Rab7-Q67L and Rab7-WT were mainly localized in Stage I melanosomes, where the full-length, immature gp100 was present (Figures 1–3), but not in Stage II and later-Stage melanosomes containing the mature gp100. Therefore, these findings allow us to speculate that Rab7 is not involved in the

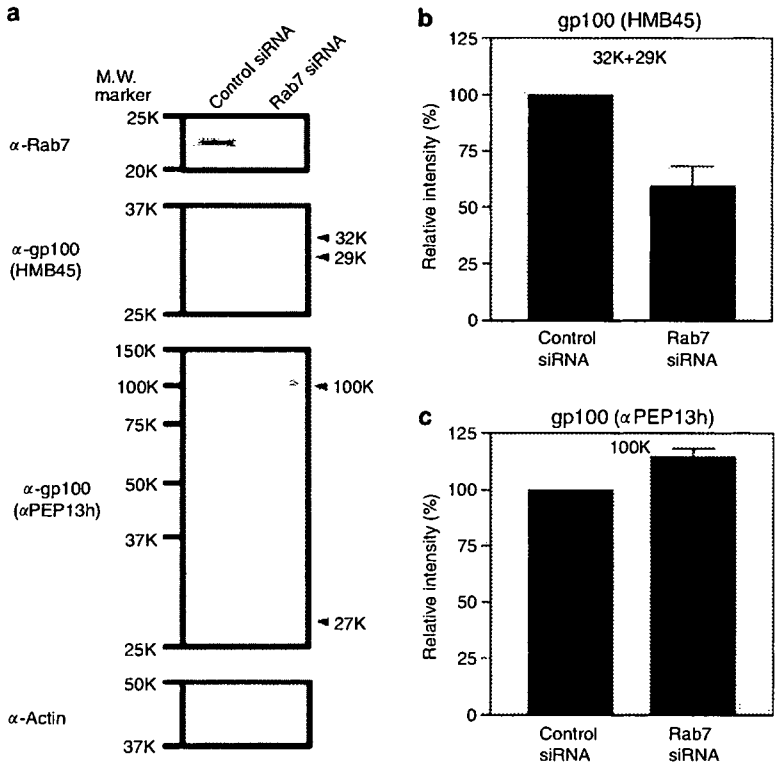

Figure 5. Downregulation of Rab7 expression with siRNA inhibits the maturation of gp100. (a) MMAc cells were transfected with control siRNA or Rab7 siRNA. After 3 days, the cells were harvested and analyzed by Western blotting using anti-Rab7 antibody, αPEP13h, HMB45, or anti-actin antibody, as indicated. Equal amounts of protein were loaded in each lane. (b and c) The band intensities of mature gp100 (32- + 29-kDa bands detected by HMB45) (b) and full-length gp100 (100-kDa band detected by αPEP13h) (c) were quantified and then normalized for those of actin. The results represent the mean ± SEM of the values obtained in four separate experiments. The value of control siRNA-transfected cells was set at 100.

later stages of gp100 maturation processes including stabilization and fibrous matrix formation. Hence, it is possible that Rab7 plays important roles in the expression of gp100 and/or early processes of its maturation such as transport to Stage I melanosomes and proteolysis there. Since the amount of full-length gp100 (precursor, 100-kDa band in Figure 4a) was not affected by the overexpression of Rab7-Q67L and Rab7-WT, it is likely that Rab7 participates in the early processes of gp100 maturation in the Stage I melanosomes but not in the regulation of its expression. Although we analyzed the subcellular localization of gp100 in MMAc cells transfected with Rab7 siRNA, no significant changes were detected (data not shown). Thus, we consider that defects in processing, instead of mistargeting, of gp100, is the most probable explanation for our results. If gp100 processing is accelerated (Figure 4), it is predicted that the levels of the full-length gp100 should be decreased. However, the amounts of the precursor, the full-length gp100, were not changed (Figure 4). As shown in Figure 5c, the amount of the full-length gp100 was slightly augmented by the Rab7 knockdown. However, this slight increase does not fully explain the marked decrease of the mature 29/32-kDa bands (Figure 5b). Although the precise mechanism is still unknown, a potential explanation of these results is that, in the maturation pathway, the cleavage step may be rate limiting. In the experiment shown in Figure 4, it is also expected that the amounts of the C-terminal proteolytic product (27-kDa band in Figure 4a, upper middle panel), which is also recognized by αPEP13h, as well as the mature forms of gp100 (32- and 29-kDa bands in Figure 4a, top panel), are simultaneously increased because of the enhanced processing (proteolysis) of the full-length gp100 (Figure 3a). Although significantly increased levels of the mature forms were detected, however, such an increase of the C-terminal 27-kDa band was not observed (data not shown). The most probable explanation of this result is that only the mature forms of gp100 are stably accumulated in melanosomes, whereas the C-terminal 27-kDa fragment is rapidly degraded (Yasumoto *et al.*, 2004).

There are two possible mechanisms for promotion of gp100 processing: (1) Rab7 enhances the transport of gp100 itself to Stage I melanosomes, where gp100 is processed, and (2) Rab7 promotes the transport of enzymes and their regulators that participate in the processing of gp100. As for the first possibility, gp100 is reported to be transported from the TGN to Stage I melanosomes directly and/or indirectly via the plasma membrane and early/late endosomes (Raposo *et al.*, 2001; Valencia *et al.*, 2006). Thus, it is possible that Rab7 associated with Stage I melanosomes promotes vesicle trafficking and membrane fusion between melanosomes and either the TGN or early/late endosomes. We previously

reported that Rab7 is involved in the transport of TYRP-1 and tyrosinase from the TGN to melanosomes (Gomez *et al.*, 2001; Hirosaki *et al.*, 2002). It is therefore interesting to speculate that there are common transport mechanisms underlying the conveyance of TYRP-1/tyrosinase and gp100 to their destination, melanosomes.

Regarding the second possibility, several factors were reported to participate in the proteolysis of gp100. For instance, pro-hormone convertase, which exists in the endoplasmic reticulum, TGN, exocytotic vesicles, endosomes, and melanosomes (Peters *et al.*, 2000; Thomas, 2002), was reported to cleave gp100 (Berson *et al.*, 2003). MART-1 interacts with gp100, and is involved in its expression, stabilization, transport, and cleavage (Hoashi *et al.*, 2005). Overexpression of myosin Ib caused a marked delay of the gp100 proteolysis (Salas-Cortes *et al.*, 2005). Thus, Rab7 may positively (pro-hormone convertase and MART-1) or negatively (myosin Ib) regulate the supply (transport) of, at least, one of these factors to melanosomes, and thereby control the gp100 processing/maturation. Further work is required to elucidate which one of these factors/mechanisms is directly responsible for the Rab7-dependent gp100 maturation.

The maturation (glycosylation) of TYRP-1 and tyrosinase occurs in the Golgi apparatus. Thus, when restricted to "maturation", the effect of Rab7 is likely to be specific for gp100. However, melanosome biogenesis consists of multiple steps such as the transport of structural and enzymatic proteins and their subsequent structural organization as well as melanin deposition. Therefore, we rather consider that Rab7 comprehensively and cooperatively regulates melanosome biogenesis by controlling the transport of TYRP-1 and tyrosinase, and the maturation (proteolytic cleavage) of gp100.

In summary, this study, which deals with the complex multistep processes of melanosome biogenesis, has provided several lines of evidence indicating that Rab7 is involved in gp100 maturation and enhances its processing in Stage I melanosomes. Rab7 plays an important role in many vesicle transport pathways. Thus, future studies exploring how Rab7 regulates gp100 maturation will provide further insight not only into melanogenesis in melanocytes *per se* but also into vesicular transport regulated by Rab7 in cells.

MATERIALS AND METHODS

Plasmid constructs

pGEM-canine Rab7 was prepared as described previously (Chavrier *et al.*, 1990; Bucci *et al.*, 1994). Rab7-Q67L (a GTPase-deficient, dominant-active mutant) and Rab7-T22N (a GDP-bound, dominant-negative mutant) were generated using the QuikChange Site-directed Mutagenesis Kit (Stratagene, La Jolla, CA). These WT and mutant cDNAs of Rab7 were fused in frame with pEYFP-C1 (Takara-Clontech, Tokyo, Japan) and p3xFLAG-CMV-7.1 (Sigma-Aldrich, Tokyo, Japan).

Cell culture and transfection

MMAc human melanoma cells were the kind gifts of Drs Tetsuya Moriuchi and Jun-ichi Hamada (Institute for Genetic Medicine, Hokkaido University School of Medicine, Sapporo, Japan). MMAc cells were maintained in Dulbecco's modified Eagle's medium (Sigma-Aldrich) containing 10% fetal bovine serum at 37 °C in an atmosphere of 5% CO_2. MMAc cells were transiently transfected with cDNAs using Effectene transfection reagent (Qiagen, Tokyo, Japan) according to the instructions from the manufacturer. Two days after transfection, cells were harvested for further analysis.

RNA interference

To silence the expression of human Rab7 (GenBank accession number: NM 004637), the following oligonucleotides (iGENE Therapeutics, Tsukuba, Japan), which had already been reported to successfully knockdown Rab7 (Jager *et al.*, 2004), were used: (5′-cgguuccagucucucggug-ag-3′) and its complementary sequence (5′-caccgagagacuggaaccg-au-3′) (nucleotides 205–223 in the open reading frame). As a negative control, the following oligonucleotides targeting green fluorescent protein, which is not expressed in mammalian cells, were used: 5′-acggcaucaaggugaacuucaagau-ag-3′ and its complementary sequence (5′-aucuugaaguucaccuugaugccgu au-3′). The annealed oligonucleotide duplex was transfected into cells using HiPerFect Transfection Reagent (Qiagen) according to the instructions from the manufacturer. Three days after transfection, cells were harvested for further analysis.

Antibodies

Anti-Rab7 rabbit polyclonal antibody was raised against the C-terminal peptide of Rab7 (KQETEVELYNEFPEPIKLDKNDRAKT SAESCSC, amino acids 175–207) (Chavrier *et al.*, 1990; Feng *et al.*, 1995; Dong *et al.*, 2004). αPEP13h (rabbit polyclonal antibody) reactive to the full-length gp100 and its truncated C-terminus was kindly provided by Dr Vincent J. Hearing (Laboratory of Cell Biology, National Cancer Institute, National Institutes of Health, Bethesda, MD). HMB45 (mouse monoclonal antibody) for the processed internal domain of gp100 was purchased from Lab Vision (Fremont, CA). Anti-LAMP-2 mouse monoclonal and anti-actin goat polyclonal antibodies were purchased from Research Diagnostics (Concord, MA) and (Santa Cruz Biotechnology, Santa Cruz, CA), respectively. Anti-FLAG M2 mouse monoclonal antibody was purchased from Sigma-Aldrich.

Western blot analysis

MMAc cells grown on 60-mm dishes were transiently transfected with siRNAs or plasmids encoding different forms of Rab7. Mock transfections were performed using empty vectors. Transfected MMAc cells were washed twice with phosphate-buffered saline (PBS). The transfected cells were lysed in 500 μl lysis buffer containing 150 mM NaCl, 20 mM Tris-HCl, pH 7.4, 1 mM EDTA, 1 mM phenylmethylsulfonyl fluoride, and protease inhibitor cocktail (one tablet/50 ml, Roche Diagnostics, Tokyo, Japan). After the cells were lysed by sonication, followed by centrifugation at 400 × *g* for 5 minutes, the supernatant was mixed with its one-fourth volume of SDS-sample buffer (125 mM Tris-HCl, pH 6.8, 10% SDS, 50% glycerol, 10% 2-mercaptoethanol, 0.005% bromophenol blue), and boiled for 5 minutes. Protein concentrations were measured using the BCA protein assay (Pierce Biotechnology, Rockford, IL). Equal amounts of protein were separated on 12% SDS-PAGE. The separated proteins were transferred to a polyvinylidene difluoride membrane (Bio-Rad Laboratories, Tokyo, Japan) and blocked with

Block Ace (Dainippon Pharmaceutical, Tokyo, Japan). The membrane was incubated with αPEP13h, HMB45, anti-actin antibody, anti-FLAG M2 antibody, or anti-Rab7 antibody in 10% Block Ace for 1 hour. The immunoreactive bands were visualized using peroxidase-conjugated anti-mouse, anti-rabbit, or anti-goat IgG antibody (Jackson ImmunoResearch Laboratories, West Grove, PA), and the ECL Plus Western blotting detection system (GE Healthcare Bio-Sciences, Piscataway, NJ). To measure the relative density of immunoreactive bands, images were scanned and analyzed by Image J software (National Institutes of Health, Bethesda, MD).

Fluorescence microscopy

MMAc cells were grown on poly-L-lysine-coated glass coverslips and transiently transfected with the control vector or cDNAs encoding Rab7-WT and its mutants fused with YFP. After 2 days, MMAc cells were washed twice with PBS and fixed with 3.7% formaldehyde in PBS for 10 minutes at room temperature. After being washed twice with PBS, the cells were permeabilized with 0.1% Triton X-100 in PBS for 5 minutes at room temperature. After being washed twice with PBS, the cells were incubated in PBS containing 2% BSA for 30 minutes at room temperature as a blocking step. The cells were then incubated in 10% Block Ace/PBS containing αPEP13h, HMB45, or anti-LAMP-2 for 1 hour at room temperature. This was followed by incubation with the corresponding secondary antibodies, that is, goat anti-rabbit IgG or goat anti-mouse IgG coupled with Alexa Fluor 594 (Molecular Probes, Eugene, OR). The coverslips were mounted using Vectashield (Vector Laboratories, Burlingame, CA). Stains in cells were observed using an inverted confocal laser scanning microscope (Zeiss LSM 510). Images were processed using Adobe Photoshop 8.0.1 (Adobe Systems, San Jose, CA).

CONFLICT OF INTEREST

The authors state no conflict of interest.

ACKNOWLEDGMENTS

This work was supported in part by grants from the Ministry of Education, Culture, Sports, Science and Technology, and Health and Labour Sciences Research. We thank Drs Tetsuya Moriuchi and Jun-ichi Hamada (Institute for Genetic Medicine, Hokkaido University, Sapporo, Japan) for providing MMAc human melanoma cells. We thank Dr Vincent J. Hearing (National Cancer Institute, National Institutes of Health, Bethesda, MD) for the kind gift of anti-gp100 antibody (αPEP13h).

REFERENCES

Berson JF, Theos AC, Harper DC, Tenza D, Raposo G, Marks MS (2003) Proprotein convertase cleavage liberates a fibrillogenic fragment of a resident glycoprotein to initiate melanosome biogenesis. *J Cell Biol* 161:521–33

Bucci C, Thomsen P, Nicoziani P, McCarthy J, van Deurs B (2000) Rab7: a key to lysosome biogenesis. *Mol Biol Cell* 11:467–80

Bucci C, Wandinger-Ness A, Lutcke A, Chiariello M, Bruni CB, Zerial M (1994) Rab5a is a common component of the apical and basolateral endocytic machinery in polarized epithelial cells. *Proc Natl Acad Sci USA* 91:5061–5

Cantalupo G, Alifano P, Roberti V, Bruni CB, Bucci C (2001) Rab-interacting lysosomal protein (RILP): the Rab7 effector required for transport to lysosomes. *EMBO J* 20:683–93

Chabrillat ML, Wilhelm C, Wasmeier C, Sviderskaya EV, Louvard D, Coudrier E (2005) Rab8 regulates the actin-based movement of melanosomes. *Mol Biol Cell* 16:1640–50

Chavrier P, Parton RG, Hauri HP, Simons K, Zerial M (1990) Localization of low molecular weight GTP binding proteins to exocytic and endocytic compartments. *Cell* 62:317–29

De Maziere AM, Muehlethaler K, van Donselaar E, Salvi S, Davoust J, Cerottini JC *et al.* (2002) The melanocytic protein Melan-A/MART-1 has a subcellular localization distinct from typical melanosomal proteins. *Traffic* 3:678–93

Dong J, Chen W, Welford A, Wandinger-Ness A (2004) The proteasome α-subunit XAPC7 interacts specifically with Rab7 and late endosomes. *J Biol Chem* 279:21334–42

Feng Y, Press B, Wandinger-Ness A (1995) Rab 7: an important regulator of late endocytic membrane traffic. *J Cell Biol* 131:1435–52

Gomez PF, Luo D, Hirosaki K, Shinoda K, Yamashita T, Suzuki J *et al.* (2001) Identification of rab7 as a melanosome-associated protein involved in the intracellular transport of tyrosinase-related protein 1. *J Invest Dermatol* 117:81–90

Harrison RE, Bucci C, Vieira OV, Schroer TA, Grinstein S (2003) Phagosomes fuse with late endosomes and/or lysosomes by extension of membrane protrusions along microtubules: role of Rab7 and RILP. *Mol Cell Biol* 23:6494–506

Hirosaki K, Yamashita T, Wada I, Jin HY, Jimbow K (2002) Tyrosinase and tyrosinase-related protein 1 require Rab7 for their intracellular transport. *J Invest Dermatol* 119:475–80

Hoashi T, Muller J, Vieira WD, Rouzaud F, Kikuchi K, Tamaki K *et al.* (2006) The repeat domain of the melanosomal matrix protein PMEL17/GP100 is required for the formation of organellar fibers. *J Biol Chem* 281:21198–208

Hoashi T, Watabe H, Muller J, Yamaguchi Y, Vieira WD, Hearing VJ (2005) MART-1 is required for the function of the melanosomal matrix protein PMEL17/GP100 and the maturation of melanosomes. *J Biol Chem* 280:14006–16

Jager S, Bucci C, Tanida I, Ueno T, Kominami E, Saftig P *et al.* (2004) Role for Rab7 in maturation of late autophagic vacuoles. *J Cell Sci* 117: 4837–48

Jimbow K, Park JS, Kato F, Hirosaki K, Toyofuku K, Hua C *et al.* (2000) Assembly, target-signaling and intracellular transport of tyrosinase gene family proteins in the initial stage of melanosome biogenesis. *Pigment Cell Res* 13:222–9

Johansson M, Lehto M, Tanhuanpaa K, Cover TL, Olkkonen VM (2005) The oxysterol-binding protein homologue ORP1L interacts with Rab7 and alters functional properties of late endocytic compartments. *Mol Biol Cell* 16:5480–92

Kuroda TS, Ariga H, Fukuda M (2003) The actin-binding domain of Slac2-a/melanophilin is required for melanosome distribution in melanocytes. *Mol Cell Biol* 23:5245–55

Meresse S, Gorvel JP, Chavrier P (1995) The rab7 GTPase resides on a vesicular compartment connected to lysosomes. *J Cell Sci* 108:3349–58

Mizuno K, Kitamura A, Sasaki T (2003) Rabring7, a novel Rab7 target protein with a RING finger motif. *Mol Biol Cell* 14:3741–52

Peters EM, Tobin DJ, Seidah NG, Schallreuter KU (2000) Pro-opiomelanocortin-related peptides, prohormone convertases 1 and 2 and the regulatory peptide 7B2 are present in melanosomes of human melanocytes. *J Invest Dermatol* 114:430–7

Pfeffer SR (1999) Transport-vesicle targeting: tethers before SNAREs. *Nat Cell Biol* 1:E17–22

Press B, Feng Y, Hoflack B, Wandinger-Ness A (1998) Mutant Rab7 causes the accumulation of cathepsin D and cation-independent mannose 6-phosphate receptor in an early endocytic compartment. *J Cell Biol* 140: 1075–89

Raposo G, Tenza D, Murphy DM, Berson JF, Marks MS (2001) Distinct protein sorting and localization to premelanosomes, melanosomes, and lysosomes in pigmented melanocytic cells. *J Cell Biol* 152:809–24

Salas-Cortes L, Ye F, Tenza D, Wilhelm C, Theos A, Louvard D *et al.* (2005) Myosin Ib modulates the morphology and the protein transport within multi-vesicular sorting endosomes. *J Cell Sci* 118:4823–32

Somsel Rodman J, Wandinger-Ness A (2000) Rab GTPases coordinate endocytosis. *J Cell Sci* 113:183–92

Stein MP, Feng Y, Cooper KL, Welford AM, Wandinger-Ness A (2003) Human VPS34 and p150 are Rab7 interacting partners. *Traffic* 4:754–71

Strom M, Hume AN, Tarafder AK, Barkagianni E, Seabra MC (2002) A family of Rab27-binding proteins. Melanophilin links Rab27a and myosin Va function in melanosome transport. *J Biol Chem* 277:25423–30

Takai Y, Sasaki T, Matozaki T (2001) Small GTP-binding proteins. *Physiol Rev* 81:153–208

Theos AC, Truschel ST, Raposo G, Marks MS (2005) The Silver locus product Pmel17/gp100/Silv/ME20: controversial in name and in function. *Pigment Cell Res* 18:322–36

Thomas G (2002) Furin at the cutting edge: from protein traffic to embryogenesis and disease. *Nat Rev Mol Cell Biol* 3:753–66

Valencia JC, Watabe H, Chi A, Rouzaud F, Chen KG, Vieira WD *et al.* (2006) Sorting of Pmel17 to melanosomes through the plasma membrane by AP1 and AP2: evidence for the polarized nature of melanocytes. *J Cell Sci* 119:1080–91

Vitelli R, Santillo M, Lattero D, Chiariello M, Bifulco M, Bruni CB *et al.* (1997) Role of the small GTPase Rab7 in the late endocytic pathway. *J Biol Chem* 272:4391–7

Wu X, Rao K, Bowers MB, Copeland NG, Jenkins NA, Hammer JA III (2001) Rab27a enables myosin Va-dependent melanosome capture by recruiting the myosin to the organelle. *J Cell Sci* 114:1091–100

Yasumoto K, Watabe H, Valencia JC, Kushimoto T, Kobayashi T, Appella E *et al.* (2004) Epitope mapping of the melanosomal matrix protein gp100 (PMEL17): rapid processing in the endoplasmic reticulum and glycosylation in the early Golgi compartment. *J Biol Chem* 279:28330–8

Zerial M, McBride H (2001) Rab proteins as membrane organizers. *Nat Rev Mol Cell Biol* 2:107–17

Original Paper

Blood Purification

Blood Purif 2007;25:483–489
DOI: 10.1159/000112516

Received: April 11, 2007
Accepted: August 4, 2007
Published online: December 17, 2007

Serum Levels of Pigmentation Markers Are Elevated in Patients Undergoing Hemodialysis

Kazutaka Murakami[a] Kazumasa Wakamatsu[b] Yukiko Nakanishi[b]
Hiroki Takahashi[a] Satoshi Sugiyama[a] Shosuke Ito[b]

[a]Department of Nephrology, School of Medicine, and [b]Department of Chemistry, School of Health Sciences, Fujita Health University, Toyoake, Aichi, Japan

Key Words
5-*S*-Cysteinyldopa · Hemodialysis · Hyperpigmentation · Pheomelanin

Abstract
Background: Diffuse hyperpigmentation is common among patients with chronic renal failure undergoing hemodialysis (HD). We have examined serum levels of 5-*S*-cysteinyldopa (5SCD, a pheomelanin precursor), pheomelanin, eumelanin, and protein-bound (PB-) 3,4-dihydroxyphenylalanine (DOPA) and PB-5SCD in HD patients. ***Methods:*** Pheomelanin and eumelanin were assayed by chemical degradation methods. ***Results:*** Serum levels of free 5SCD in HD patients (n = 16) were 9-fold higher than in healthy controls (n = 16). Levels of pheomelanin in HD patients were 2.6-fold higher than in controls, while levels of eumelanin did not differ between HD patients and controls. Levels of PB-DOPA and PB-5SCD in HD patients were approximately 1.5-fold higher than in controls. Serum levels of free 5SCD were positively correlated to the duration of HD therapy. ***Conclusions:*** The high constitutive levels of free 5SCD, pheomelanin, and PB-DOPA in the blood may be deteriorating in HD patients through the production of reactive oxygen species.

Introduction

Diffuse pigmentation is common among patients with chronic renal failure who are undergoing hemodialysis (HD) [1]. The mechanism(s) of skin hyperpigmentation in HD patients remain unclarified, but the accumulation of middle-molecular-weight molecules such as lipochromes, urochromic pigments, and α-melanocyte-stimulating hormone has been implicated [2].

Melanin pigments are classified into two types: brown to black eumelanin and yellow to reddish-brown pheomelanin. Eumelanin is a heterogeneous polymer derived from the oxidation of 5,6-dihydroxyindoles which arise from the oxidation of tyrosine by tyrosinase, while pheomelanin is a sulfur-containing polymer formed by oxidation of 5-*S*-cysteinyldopa (5SCD) and 2-*S*-cysteinyldopa (2SCD) which result from the intervention of cysteine with the eumelanin pathway [3] (fig. 1). Pheomelanin is known to act as a photosensitizer generating reactive oxygen species upon UV exposure [4].

In chronic renal failure as well as other diseases, oxidative stress results from the oxidative interaction of proteins, lipids, carbohydrates, DNA, and antioxidant substrates with reactive oxygen species such as hydroxyl radicals, superoxide radicals and hydrogen peroxide [5–7]. Protein-bound 3,4-dihydroxyphenylalanine (PB-DOPA) is formed when hydroxyl radicals react with protein ty-

KARGER
Fax +41 61 306 12 34
E-Mail karger@karger.ch
www.karger.com

0253–5068/07/0256–0483$23.50/0

Accessible online at:
www.karger.com/bpu

Shosuke Ito, PhD
Department of Chemistry, Fujita Health University School of Health Sciences
1-98 Dengakugakubo, Kutsukake-cho
Toyoake, Aichi 470-1192 (Japan)
Tel. +81 562 93 2595, Fax +81 562 4595, E-Mail sito@fujita-hu.ac.jp

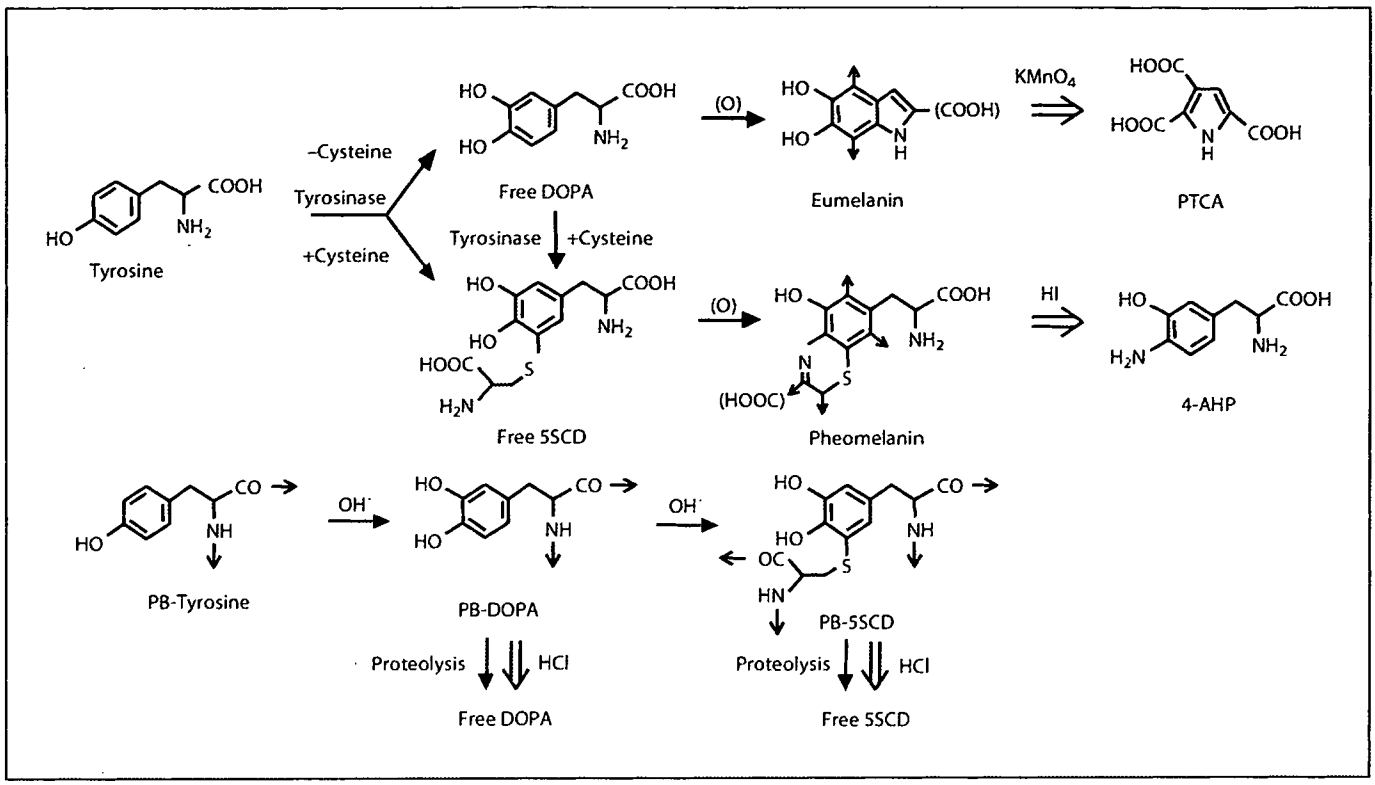

Fig. 1. Metabolic pathways for the production of eumelanin, pheomelanin, and PB-DOPA and PB-5SCD. Thin and thick arrows indicate metabolic pathways and chemical degradations, respectively. Free DOPA and 5SCD are precursors of eumelanin and pheomelanin, respectively. PTCA is produced by permanganate oxidation of eumelanin, while 4-AHP is from pheomelanin by hydriodic acid reductive hydrolysis. PB-tyrosine (tyrosine residue in protein) is oxidized to give PB-DOPA followed by PB-5SCD. Proteolysis of PB-DOPA and PB-5SCD affords free DOPA and 5SCD in vivo. Acid hydrolysis (chemical degradation) affords the same amino acids.

rosine residues [8]. Further oxidation of PB-DOPA by hydroxyl radicals may lead to the production of protein-bound (PB)-5SCD by combining DOPAquinone residue with cysteine residue [9]. Some HD patients were found to have elevated levels of PB-DOPA [8]. Pigmentation normally takes place within melanosomes, specific organelles present in melanocytes, and proceeds under the control of many pigmentary genes, including tyrosinase [10]. However, under some pathophysiological conditions such as UV exposure, pigmentation may also proceed by the action of reactive oxygen species on melanin precursors [11]. PB-DOPA and PB-5SCD in the blood may become a source of melanin through proteolic hydrolysis to free DOPA and 5SCD and their subsequent oxidation [12].

In this study, we analyzed serum levels of free 5SCD, pheomelanin, eumelanin, PB-DOPA, and PB-5SCD as markers of pigmentation in HD patients (fig. 1). We also evaluated whether HD treatment effectively removes these metabolites. We applied methods recently developed by us to analyze pheomelanin and eumelanin in serum [13, 14].

Materials and Methods

Subjects and Blood Collection

Patients on long-term HD therapy were recruited from the HD unit of our University hospital. The 16 patients studied were 66.0 ± 6.1 years of age and consisted of 9 males and 7 females. The duration of HD therapy was 103 ± 65 months. The causes of end-stage renal disease were diabetic nephropathy in 6 patients, glomerulonephritis in 6 patients, nephrosclerosis in 2 patients and antineutrophil cytoplasmic antibody-related nephritis in 2 patients. All patients were in a stable condition for at least 6 months and were undergoing HD 3 times a week for 4 h per dialysis session to maintain a minimum Kt/V urea index of 1.2 per session (1.45 ± 0.23 for 16 patients). The patients were treated with hollow-fiber dialyzers equipped with polysulfone (10 patients on PS-UW, Fresenius Kawasumi Co., Tokyo, Japan, and 6 patients on ASP-SA, Asahi Kasei Medical Co., Tokyo, Japan). For all patients

studied, standard bicarbonate-based dialysates were used with ultrapure water (<5 endotoxin units/l).

Blood samples from HD patients were obtained just before and immediately after an HD session from the arterial dialyzer tubing. In addition, we collected blood samples from the arterial and the venous dialyzer tubing at 1 h after the start of the HD session. Collection was done from November 2005 to January 2006. Blood samples were allowed to coagulate, and sera were separated by centrifugation and stored at -70°C for up to 3 months until analysis. Analytes were known to be stable under these storage conditions. Informed consent was obtained from all patients, and the protocol was approved by the University hospital committee.

Blood samples from 16 healthy controls were collected in April, 2006. They were aged 63.1 ± 3.6 years ($p > 0.05$ from HD patients) and consisted of 8 males and 8 females ($p > 0.05$).

Determination of Serum Levels of Free 5SCD, Pheomelanin, Eumelanin, PB-DOPA and PB-5SCD

Determination of serum levels of free 5SCD was performed using HPLC with electrochemical detection as previously reported [15]. Determination of serum pheomelanin was performed using HPLC with electrochemical detection as previously described [13]. Thus, pheomelanin was converted to 4-amino-3-hydroxyphenylalanine (4-AHP) by reductive hydrolysis with hydriodic acid (fig. 1). Determination of serum eumelanin was performed using HPLC with ultraviolet detection as previously reported [14]. Thus, eumelanin was oxidized to the specific marker pyrrole-2,3,5-tricarboxylic acid (PTCA) by acidic permanganate oxidation (fig. 1).

PB-DOPA and PB-5SCD (fig. 1) were analyzed by the method of Sutherland et al. [8] with some modifications. Prior to analysis, serum samples were filtered through Micro-Spin filter tubes (0.45 μm pore size; Alltech Associates, Inc., Deerfield, Ill., USA) by centrifugation to remove any insoluble, fiber-like precipitate. A 20-μl aliquot of each serum sample was mixed with 980 μl water in an Eppendorf tube, to which 140 μl of 72% (w/v) trichloroacetic acid was added, and the mixture was vortex mixed. Each mixture was kept on ice for 15 min and then centrifuged. After removal of the supernatant, each pellet was washed with 1 ml chloroform:methanol (1:1, v/v). After vortex mixing and centrifugation, each pellet was washed with 1 ml diethyl ether. After centrifugation and aspiration, the residual ether was removed and each pellet was transferred to a sealed-capped tube with 300 μl 6 M HCl containing 5% thioglycolic acid and 1% phenol. The tube was purged with a stream of argon, then sealed and heated at 110°C for 16 h. A standard solution of 10 μl DOPA and 5SCD (5 μmol/l each) was heated similarly. After cooling, each hydrolysate was mixed with 10 μl of an internal standard solution (methyl-5SCD, 15 μmol/l), extracted twice with 1 ml diethyl ether, and treated with alumina to extract catecholic compounds as follows [see 14]. A 100-μl aliquot of each hydrolysate was transferred into an Eppendorf tube containing 50 mg acid-washed alumina and 200 μl 1% $Na_2S_2O_5$ – 1% EDTA.2Na. To the mixture, 500 μl 2.7 M Tris. HCl – 2% EDTA.2Na (pH 9.0) was added and immediately mixed vigorously for 5 min on a microtube mixer. After centrifugation, the aqueous layer was removed by aspiration, and the remaining alumina was washed with 1 ml water three times. DOPA and 5SCD were then eluted with 100 μl 0.4 M $HClO_4$ by shaking for 2 min. A 30-μl aliquot of each $HClO_4$ extract was injected into the HPLC system to assay free 5SCD as described in Wakamatsu and Ito [15]. A modification from the previous HPLC conditions was that the column was maintained at room temperature (25°C). Under these hydrolytic conditions, 5SCD was significantly converted to the dihydrobenzothiazine as described in Costantini et al. [16]. Therefore, we calculated the 5SCD value as the sum of 5SCD and its dihydrobenzothiazine derivative. The intra-assay variation of the assays in pooled sera (n = 5) was 538 ± 72 nmol/l for PB-DOPA and 62 ± 6.3 nmol/l for PB-5SCD, the coefficients of variation (CV) being 13.4 and 10.2%, respectively. The inter-assay variation (n = 5) was 544 ± 74 nmol/l for PB-DOPA and 56 ± 8.4 nmol/l for PB-5SCD, the CV being 13.6 and 15.0%, respectively. The % recovery of 50 pmol each of DOPA and 5SCD added to 20 μl of pooled sera (n = 5) was 97.3 ± 5.7% and 101.1 ± 7.3%, respectively.

Statistical Analysis

Statistical testing was carried out using JMP 5.0 for Macintosh. Differences were analyzed for statistical significance using the nonparametric Mann-Whitney U test (fig. 2). Paired t tests were applied for the comparison of values at the inlet and outlet (fig. 3). Pearson's correlation test was used for correlations of variables (fig. 3). $p < 0.05$ was considered significant.

Results

Levels of pigmentation markers were compared between the sera of 16 HD patients just before a HD session and 16 healthy controls. Free 5SCD is a precursor of pheomelanin, while 4-AHP and PTCA are specific degradation products of pheomelanin and eumelanin, respectively. Thus, 5SCD, 4-AHP and PTCA serve as pigmentation markers. Figure 2a shows that serum levels of free 5SCD were elevated 9-fold in HD patients compared with controls (37.9 ± 12.5 vs. 4.1 ± 1.5 nmol/l). Similarly, levels of pheomelanin (as 4-AHP) in HD patients were 2.5 times higher than in controls (219 ± 81 vs. 85 ± 43 nmol/l; fig. 2b). In contrast, levels of serum eumelanin (as PTCA) did not show any difference between HD patients and controls (28.3 ± 13.4 vs. 26.5 ± 14.6 nmol/l; fig. 2c). PB-DOPA and PB-5SCD are proteins modified by the attack of hydroxyl radicals. Levels of PB-DOPA and PB-5SCD were about 1.5 times higher than the respective controls (789 ± 428 vs. 506 ± 152; 120 ± 53 vs. 89 ± 17 nmol/l; fig. 2d, e).

Changes in serum levels of free 5SCD during an HD session were then examined. As shown in table 1, during a 4-hour HD session, serum levels of free 5SCD were significantly decreased to one fourth the original levels. Nevertheless, the mean level of 10.5 ± 3.2 nmol/l at 4 h was still much higher than the control level of 4.1 ± 1.5 nmol/l. Table 1 also shows that serum levels of free 5SCD at 1 h of the HD session were decreased 6-fold during one passage through the dialyzer. Other 3 markers were ex-

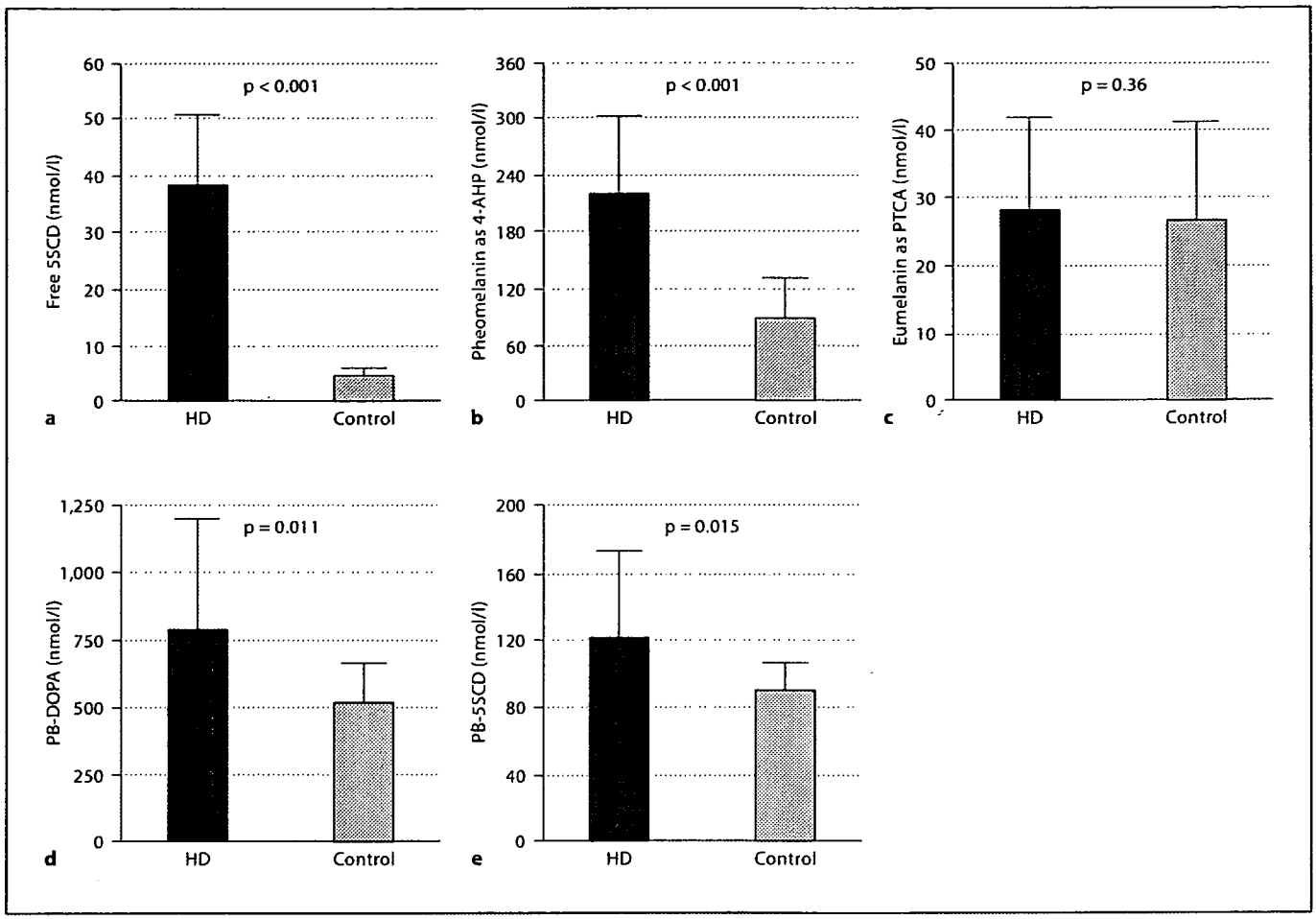

Fig. 2. Comparison of serum markers between HD patients just before an HD session and controls: **a** free 5SCD, **b** pheomelanin as 4-AHP, **c** eumelanin as PTCA, **d** PB-DOPA, and **e** PB-5SCD. Bars represent means ± SD for 16 HD patients and 16 controls.

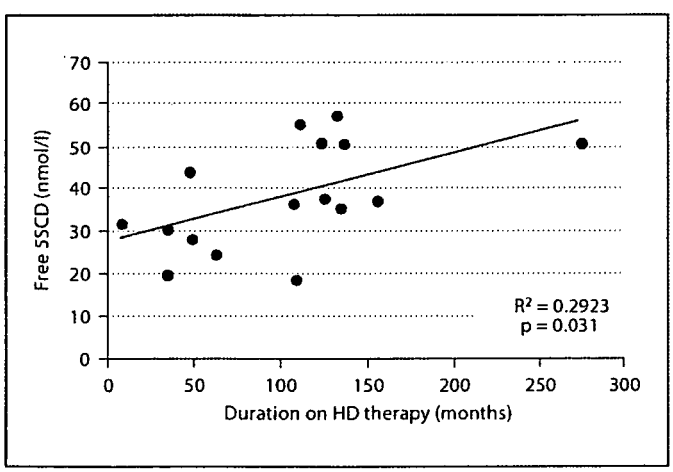

Fig. 3. Correlation between serum levels of free 5SCD and the duration of HD treatment in 16 HD patients.

amined for removal during a 4-hour HD session. Pheomelanin and PB-5SCD showed small, but significant increases by 61 and 22%, respectively. The same markers were also examined for removal during one passage through the dialyzer. Pheomelanin, PB-DOPA, and PB-5SCD did not show any change during one passage.

Correlations among serum levels of the 5 markers in HD patients were next examined. An inverse, weak correlation ($R = -0.491$, $p = 0.054$) was found between serum levels of free 5SCD and pheomelanin. This suggests a possibility that the oxidation of 5SCD to pheomelanin may occur in the circulation in HD patients. No significant correlation was found between any other combinations of the 5 markers.

The correlation of serum levels of the 5 markers with the duration of HD therapy was then examined. Figure 3

Table 1. Changes in serum levels of the 5 markers during an individual HD session

Marker	Predialysis	1 h dialysis at dialyzer inlet	1 h dialysis at dialyzer outlet	4 h dialysis
Free 5SCD	37.9 ± 11.2	22.2 ± 7.1 (<0.001)*	3.4 ± 1.5 (<0.001)**	10.5 ± 3.2 (<0.001)***
Pheomelanin as 4-AHP	219 ± 81	312 ± 204 (0.018)	292 ± 191 (0.23)	352 ± 268 (0.016)
PB-DOPA	789 ± 428	816 ± 449 (0.40)	865 ± 383 (0.29)	915 ± 405 (0.13)
PB-5SCD	120 ± 53	152 ± 134 (0.068)	132 ± 83 (0.14)	146 ± 90 (0.036)

Serum levels are expressed in nmol/l and as mean ± SD for 16 patients. Eumelanin was not measured during the HD session.
* p values between the serum levels at predialysis and 1 h after dialysis.
** p values between the serum levels 1 h after dialysis at the dialyzer inlet and outlet.
*** p values between the serum levels at predialysis and 4 h after dialysis.

shows a positive correlation (R = 0.541, p = 0.031) of serum levels of free 5SCD with the duration of HD therapy. No significant correlation was found between the duration of HD therapy and any of the other 4 markers, R values being −0.228, 0.170, 0.323, and −0.473 for pheomelanin, eumelanin, PB-DOPA, and PB-5SCD, respectively.

Discussion

Diffuse hyperpigmentation is common among HD patients. A recent study by Lai et al. [1] showed that on the abdomen, i.e. a non-sun-exposed area, the skin is significantly darker in patients with end-stage renal disease than in healthy controls. Generalized melanosis is also occasionally seen in patients with end-stage malignant melanoma [17, 18]. It has been shown that melanoma patients with generalized melanosis excrete trichochromes, a dimeric pheomelanic pigment, in their urine [17] and contain high levels of 5SCD and eumelanin-related metabolites in their sera [18]. Those patients were shown to deposit melanin granules in their skin.

In HD patients, there has been no report examining the chemical properties of melanin deposited in the skin. The present study shows that serum levels of pheomelanin (as 4-AHP) are significantly elevated in HD patients compared with healthy controls, whereas levels of eumelanin (as PTCA) are not elevated at all. It is thus expected that pheomelanin is deposited in the skin because high concentrations of pheomelanin circulate during several years while patients are treated with HD therapy. We previously showed that serum levels of pheomelanin are much elevated in melanoma patients with metastases and correlate with levels of free 5SCD [13]. These results indicate that in melanoma patients, both free 5SCD and pheomelanin are produced in melanoma cells and are secreted into the blood. On the other hand, it is assumed that in HD patients, pheomelanin is produced by oxidation of free 5SCD in the circulation because patients are exposed to high oxidative stress [5–7]. In support of this assumption, free 5SCD was shown to be oxidized by hydrogen peroxide-peroxidase, superoxide radicals, and hydroxyl radicals [19]. Plasma α-MSH levels in HD patients were shown to be elevated compared with controls [2]. However, this is not likely a direct cause for the higher levels of free 5SCD (and pheomelanin) in HD patients, because the increase is rather small, ca. 30%.

During one passage through the dialyzer, free 5SCD was removed to one sixth the original level and its level became lower than the control level. However, this removal was not sufficiently effective, because even after the 4-hour HD session, serum levels of free 5SCD were still much higher than in healthy controls. The remaining high level must result from dilution with high levels in the total blood pool. Pheomelanin was not removed at all due to its high molecular weight, which probably results from its being bound to proteins.

Patients on long-term HD therapy suffer from increased levels of oxidative stress [5–7]. Although the precise mechanisms of oxidative stress have not been definitely elucidated, the interaction of blood with nonbiological materials of the extracorporeal circuit is considered to be one main source of extra-oxidative stress. The process of HD can activate polymorphonuclear leukocytes to produce reactive oxygen species [20, 21]. In the present study, levels of pheomelanin and PB-5SCD were significantly increased after a 4-hour HD session. Although the exact mechanism for this increase is not clear, the increase could be ascribed to the elevated generation of reactive oxygen species during HD session

[20, 21] and/or the removal of excess water from the blood.

PB-DOPA and PB-5SCD can be produced by the attack of hydroxyl radicals on the tyrosine residues in protein [8, 9]. Thus, PB-DOPA and PB-5SCD could serve as markers of oxidative stress [8]. However, the actual usefulness of these markers is hampered by the fact that they are susceptible to further oxidation [22]. In fact, PB-DOPA levels in HD patients were much lower than those expected from fluorescence derived from DOPA, suggesting the oxidative modification of PB-DOPA [8].

The duration on HD therapy was found to correlate positively with levels of protein carbonyl group [6] and oxidized low-density lipoprotein [7], but negatively with levels of protein sulfhydryl groups [6] and the antioxidants α-tocopherol and ubiquinol [5]. These correlations should be ascribed to the increased levels of oxidative stress in HD patients. The present study shows that levels of free 5SCD are positively correlated to the duration on HD therapy. In melanocytes, free 5SCD is produced by the action of tyrosinase through the participation of cysteine [3]. However, it appears that non-enzymic pathways must exist that lead to the production of 5SCD, as exemplified by the presence of 5SCD in the urine of albino patients and in albino mice (which have no functional tyrosinase) [23, 24]. One possible source of free 5SCD in the blood is PB-5SCD that gives rise to free 5SCD after proteolysis (fig. 1) [9, 12]. In this connection, it should be noted that increased protein degradation is, at least in part, mediated by the HD-associated inflammatory response [25].

Finally, implications of the present findings are discussed in terms of adverse effects of the metabolites analyzed. Constitutive skin pigmentation dramatically affects the incidence of skin cancer. Fair-skinned individuals are more susceptible to UV-induced skin damage than are individuals with darker skin, resulting in a 10- to 100-fold higher frequency of skin cancer [4]. Eumelanin is believed to protect cutaneous cells by absorbing harmful UV radiation and by scavenging reactive oxygen species [11]. In contrast, it appears that pheomelanin is phototoxic since it produces reactive oxygen species upon UV radiation and induces apoptosis in adjacent cells [4]. It should be emphasized that the production of superoxide radicals from pheomelanin may occur even in the absence of UV radiation [26]. The presence of high levels of pheomelanin in the serum (and possibly in the skin) may thus cause deteriorating effects on HD patients. The pheomelanin precursor, free 5SCD, has also been shown to produce reactive oxygen species in vitro [27]. Although the serum level of free 5SCD concentration is still very low, 37.9 nmol/l, in order to produce any acute effects in HD patients, the long-time exposure to the high levels of free 5SCD might add to the adverse effects of other uremic toxins. Thus, more extensive removal of circulating free 5SCD and subsequent suppression of pheomelanin accumulation is desirable in HD patients. In addition, PB-DOPA at 500 nmol/l was found to exert oxidative damage on DNA in the presence of transition metal ions, especially copper, in vitro [28]. This concentration range is equivalent to the level seen in HD patients. Thus, additional oxidative damage should be considered in HD patients due to the presence of high levels of PB-DOPA (and possibly PB-5SCD).

In conclusion, the present study shows that serum levels of free 5SCD and pheomelanin are significantly elevated in the sera of HD patients compared with controls. These results suggest the possibility that pheomelanin accumulates in the skin of HD patients due to the high circulating levels of free 5SCD, although this possibility awaits actual measurements of pheomelanin in the skin of HD patients compared with control subjects [29]. Finally, the high constitutive levels of free 5SCD, pheomelanin, and PB-DOPA (and possibly PB-5SCD) in the blood may be deteriorating in HD patients through the production of reactive oxygen species.

Acknowledgements

This study was supported in part by a Grant-in-Aid for Scientific Research (No. 18591262) from the Ministry of Education, Culture, Sports, Science and Technology of Japan to K.W. and S.I.

References

1 Lai CF, Kao TW, Tsai TF, Chen HY, Huang KC, Wu MS, Wu KD: Quantitative comparison of skin colors in patients with ESRD undergoing different dialysis modalities. Am J Kidney Dis 2006;48:292–300.

2 Airaghi L, Garofalo L, Cutuli MG, Delgado R, Carlin A, Demitri MT, Badalamenti S, Graziani G, Lipton JM, Catania A: Plasma concentrations of α-melanocyte-stimulating hormone are elevated in patients on chronic haemodialysis. Nephrol Dial Transplant 2000;15:1212–1216.

3 Ito S: A chemist's view of melanogenesis. Pigment Cell Res 2003;16:230–236.

4 Takeuchi S, Zhang W, Wakamatsu K, Ito S, Hearing VJ, Kraemer KH, Brash DE: Melanin acts as a potent UVB photosensitizer to cause an atypical mode of cell death in murine skin. Proc Natl Acad Sci USA 2004;101:15076–15081.

5 Nguyen-Khoa T, Massy ZA, De Bandt JP, Kebede M, Salama L, Lambrey G, Witko-Sarsat V, Druek TB, Lacour B, Thevenin M: Oxidative stress and haemodialysis: role of inflammation and duration of dialysis treatment. Nephrol Dial Transplant 2001;16:335–340.
6 Köken T, Serteser M, Kahraman A, Gökçe Ç, Demir S: Changes in serum markers of oxidative stress with varying periods of haemodialysis. Nephrology 2004;9:77–82.
7 Shirai S, Ominato M, Shimazu T, Toyama K, Ogimoto G, Fujino T, Yasuda T, Sato T, Maeba T, Owada S, Kimura K: Imbalance between production and scavenging of hydroxyl radicals in patients maintained on hemodialysis. Clin Exp Nephrol 2005;9:310–314.
8 Sutherland WH, Gieseg SP, Walker RJ, de Jong SA, Firth CA, Scott N: Serum protein-bound 3,4-dihydroxyphenylalanine and related products of protein oxidation and chronic hemodialysis. Ren Fail 2003;25:997–1009.
9 Ito S, Jimbow K, Kato T, Kiyota M, Fujita K: Protein-bound dopa and 5-*S*-cysteinyldopa in non-melanogenic tissues. Acta Derm Venereol 1983;63:463–467.
10 Bennett DC, Lamoreux ML: The color loci of mice: a genetic century. Pigment Cell Res 2003;16:333–344.
11 Kadekaro AL, Wakamatsu K, Ito S, Abdel-Malek ZA: Cutaneous photoprotection and melanoma susceptibility: reaching beyond melanin content to the frontiers of DNA repair. Front Biosci 2006;11:2157–2173.
12 Rodgers KJ, Hume PM, Dunlop RA, Dean RT: Biosynthesis and turnover of DOPA-containing proteins by human cells. Free Radic Biol Med 2004;37:1756–1764.
13 Wakamatsu K, Yokochi M, Naito A, Kageshita T, Ito S: Comparison of phaeomelanin and its precursor 5-*S*-cysteinyldopa in the serum of melanoma patients. Melanoma Res 2003;13:357–363.
14 Wakamatsu K, Takasaki A, Kågedal B, Kageshita T, Ito S: Determination of eumelanin in human urine. Pigment Cell Res 2006;19:163–169.
15 Wakamatsu K, Ito S: Improved HPLC determination of 5-*S*-cysteinyldopa in serum. Clin Chem 1994;40:495–496.
16 Costantini C, Crescenti O, Prota G, Palumbo A: New intermediates of phaeomelanogenesis in vitro beyond 1,4-benzothiazine stage. Tetrahedron 1990;46:6831–6838.
17 Rorsman H, Agrup P, Carlen B, Hansson C, Jonsson N, Rosengren E, Tegner E: Trichochromuria in melanosis of melanoma. Acta Derm Venereol 1986;66:468–473.
18 Tsukamoto K, Furue M, Sato Y, Takayama O, Akusu O, Ohtake N, Wakamatsu K, Ito S, Tamaki K, Shimada G: Generalized melanosis in metastatic malignant melanoma: the possible role of DOPAquinone metabolites. Dermatology 1998;197:338–342.
19 Ito S, Fujita K: Oxygen-dependent conjugation of dopa with cysteine catalysed by iron-EDTA complex. Biochem Pharmacol 1984;33:2193–2197.
20 Yang CC, Hsu SP, Wu MS, Hsu SM, Chien CT: Effects of vitamin C infusion and vitamin E-coated membrane on hemodialysis-induced oxidative stress. Kidney Int 2006;69:706–714.
21 Yoon JW, Pahl MV, Vaziri ND: Spontaneous leukocyte activation and oxygen-free radical generation in end-stage renal disease. Kidney Int 2007;71:167–172.
22 Davies MJ, Fu S, Wang H, Dean RT: Stable markers of oxidant damage to proteins and their application in the study of human disease. Free Radic Biol Med 1999;27:1151–1163.
23 Westerhof W, Pavel S, Kammeyer A, Besenberg FD, Cormane R: Melanin-related metabolites as markers of the skin pigmentary system. J Invest Dermatol 1987;95:78–81.
24 Ekelund MC, Carstam R, Hansson C, Rorsman H, Rosengren E: Urinary excretion of 5-*S*-cysteinyldopa and 6-hydroxy-5-methoxyindole-2-carboxylic acid: differences between pigmented and albino mice. Acta Derm Venereol 1985;65:437–439.
25 Ikizier TA: Effects of hemodialysis on protein metabolism. J Ren Nutr 2005;15:39–43.
26 Ye T, Hong L, Garguilo J, Pawlak A, Edwards GS, Nemanich RJ, Sarna T, Simon JD: Photoionization thresholds of melanins obtained from free electron laser-photoelectron emission microscopy, femtosecond transient absorption spectroscopy and electron paramagnetic resonance measurements of oxygen photoconsumption. Photochem Photobiol 2006;82:733–737.
27 Spencer JP, Whiteman M, Jenner P, Halliwell B: 5-*S*-Cysteinyl-conjugates of catecholamines induce cell damage, extensive DNA base modification and increases in caspase-3 activity in neurons. J Neurochem 2002;81:122–129.
28 Morin B, Davis MJ, Dean RT: The protein oxidation product 3,4-dihydroxyphenylalanine (DOPA) mediates oxidative DNA damage. Biochem J 1998;330:1059–1067.
29 Wakamatsu K, Ito S, Rees JL: Usefulness of 4-amino-3-hydroxyphenylalanine as a specific marker of pheomelanin. Pigment Cell Res 2002;15:225–232.

4-*S*-Cysteaminylphenol-loaded magnetite cationic liposomes for combination therapy of hyperthermia with chemotherapy against malignant melanoma

Akira Ito,[1] Masatake Fujioka,[2] Tatsuro Yoshida,[2] Kazumasa Wakamatsu,[3] Shosuke Ito,[3] Toshiharu Yamashita,[4] Kowichi Jimbow[4] and Hiroyuki Honda[2,5]

[1]Department of Chemical Engineering, Faculty of Engineering, Kyushu University, 744 Mototoka, Nishi-ku, Fukuoka 819-0395; [2]Department of Biotechnology, School of Engineering, Nagoya University, Furo-cho, Chikusa-ku, Nagoya 464-8603; [3]Department of Chemistry, Fujita Health University School of Health Sciences, Toyoake, Aichi 470-1192; [4]Department of Dermatology, Sapporo Medical University School of Medicine, South 1 West 17, Chuo-ku, Sapporo 060-8556, Japan

(Received June 28, 2006/Revised October 26, 2006/Accepted October 31, 2006/Online publication December 22, 2006)

Tyrosine analogs are good candidates for developing melanoma chemotherapies because melanogenesis is inherently toxic and expressed uniquely in melanocytic cells. The sulfur homolog of tyrosine, 4-*S*-cysteaminylphenol (4-*S*-CAP), was shown to be a substrate of melanoma tyrosinase and can cause selective cytotoxicity of melanocytes and melanoma cells. Previously, in order to improve the adsorption of magnetite nanoparticles to target cell surfaces, and generate heat in an alternating magnetic field (AMF) for cancer hyperthermia, we produced hyperthermia using magnetite cationic liposomes (MCL) that have a positive charge at the liposomal surface. In the present study, we constructed 4-*S*-CAP-loaded MCL (4-*S*-CAP/MCL), which act as a novel modality, combining melanoma-specific chemotherapy by 4-*S*-CAP with intracellular hyperthermia mediated by MCL. The 4-*S*-CAP/MCL exerted 4-*S*-CAP-mediated anticancer effects on B16 melanoma cells *in vitro* and *in vivo*. Moreover, after intratumoral injection of 4-*S*-CAP/MCL *in vivo*, the melanoma nodules were heated to 45°C under an AMF. Significantly higher therapeutic effects were observed in mice treated with the combination therapy mediated by 4-*S*-CAP/MCL plus AMF irradiation compared with mice treated with 4-*S*-CAP/MCL alone (without AMF) or mice treated with hyperthermia alone (MCL + AMF irradiation). These results suggest that this novel therapeutic tool is applicable to the treatment of malignant melanoma. (*Cancer Sci* 2007; 98: 424–430)

Hyperthermia is a promising approach to cancer therapy and has been used for many years to treat a wide variety of tumors in both experimental animals and patients.[1] In Japan, the most commonly used heating method in clinical settings is capacitive heating using a radiofrequency electric field.[2] An unavoidable technical problem with hyperthermia is the difficulty in heating only the local tumor region to the intended temperature without damaging the surrounding healthy tissue. Specifically, heating tumors by capacitive heating using a radiofrequency electric field is difficult because various factors, such as tumor size, position of electrodes, and adhesion of electrodes at uneven sites, influence the heating characteristics. Hyperthermia produced by heating mediators is a promising approach for specifically heating tumors without damaging normal tissues.[3] Magnetite nanoparticles have been used for hyperthermia treatment in an attempt to overcome this obstacle.[4–6] If magnetite nanoparticles can be made to accumulate only in tumor tissue, cancer-specific hyperthermia can be achieved by generating heat in an alternating magnetic field (AMF) due to hysteresis loss. In order to test this hypothesis, we developed magnetite cationic liposomes (MCL) as mediators of intracellular hyperthermia.[7–9] These cationic liposomes exhibit improved adsorption and accumulation in tumor cells, and have 10-fold higher affinity for tumor cells than neutrally charged magnetoliposomes,[7] thus suggesting that MCL are superior mediators of hyperthermia. We previously demonstrated the efficacy of MCL-mediated hyperthermia in animals with several cell lines, including T-9 rat glioma,[9] Os515 hamster osteosarcoma,[10] MM46 mouse mammary carcinoma,[11] PLS 10 rat prostate cancer,[12] and VX-7 squamous cell carcinoma in rabbit tongue.[13] Although MCL-mediated hyperthermia was found to be very effective for inducing complete tumor regression in transplantable tumor models, more powerful therapies are highly desired for cancer patients with malignancy.

Among the various forms of neoplasmas of the skin, malignant melanoma is the most invasive tumor. Various medical therapies, such as surgery, chemotherapy, radiotherapy and immunotherapy, are commonly used in the treatment of melanoma patients; however, none of these has proved sufficiently effective. Therefore, an effective protocol for the prevention and treatment of melanoma is needed urgently. Given this background, the combination of chemotherapy with MCL-mediated hyperthermia can be considered a possible strategy, because both magnetite nanoparticles and anticancer drugs can be encapsulated simultaneously into a liposome.

Tyrosine analogs are good candidates for developing melanoma chemotherapy because melanogenesis is inherently toxic and uniquely expressed in melanocytic cells. We introduced the use of phenolic thioether analogs of tyrosine for targeted melanoma chemotherapy based on the idea that the incorporation of sulfur would render the phenolics more cytotoxic by increased lipophilicity leading to increased uptake by cells, thus making them better substrates for tyrosinase.[14] Therefore, we synthesized the sulfur homolog of tyrosine, 4-*S*-cysteaminylphenol (4-*S*-CAP), in order to develop a targeted chemotherapy for malignant melanoma.[14,15] 4-*S*-CAP was found to be a substrate of melanoma tyrosinase and can cause selective cytotoxicity of melanocytes and melanoma cells.[16] In the present study, we constructed 4-*S*-CAP-loaded magnetite cationic liposomes (4-*S*-CAP/MCL) and investigated the feasibility of using them for combined melanoma-targeted chemotherapy and tumor-specific hyperthermia.

Materials and Methods

Cell lines and animal models. Mouse B16 melanoma cells were cultured in Dulbecco's modified Eagle's medium (Gibco BRL, Gaithersburg, MD, USA), supplemented with 10% fetal calf serum, 0.1 mg/mL streptomycin sulfate and 100 IU/mL potassium penicillin G. Normal human dermal fibroblasts (NHDF) were provided as frozen cells after primary culture by the supplier (Kurabo, Osaka, Japan), and were cultured in commercially available growth media (Medium106S; Kurabo) at 37°C in a humidified atmosphere of CO_2 and 95% air.

[5]To whom correspondence should be addressed. E-mail: honda@nubio.nagoya-u.ac.jp

doi: 10.1111/j.1349-7006.2006.00382.x

To prepare tumor-bearing mice, 8×10^5 B16 melanoma cells were injected subcutaneously into the right flank of C57BL/6 mice, which were anesthetized by intraperitoneal injection of pentobarbital (50 mg/kg bodyweight). Melanoma nodules that had grown to 5 mm in diameter were used for experiments. Tumor diameter was measured using calipers and the average size was determined by applying the following formula:

$$\text{Tumor size} = 0.5 \times (\text{length} + \text{width}),$$

where length and width were measured in mm.

Animal experiments were carried out according to the principles described in the 'Guide for the Care and Use of Laboratory Animals' prepared under the direction of the Prime Minister of Japan.

Analysis of the combined effect of 4-*S*-CAP and hyperthermic treatment. B16 cells were plated in six-well cell culture plates at 4×10^4 cells/well with experimental media containing 4-*S*-CAP at a concentration of 50 μM. The cells were then treated with hyperthermic treatment using a water bath. Hyperthermic treatment of cultured cells was carried out as in our previous report.[17] Briefly, the cells were heated to 42.5°C for 60 min by direct immersion of cell culture dishes in a temperature-controlled water bath. The temperature of the medium increased quickly and reached the intended temperature within 5 min. The temperature of the medium was monitored using a fiber optic thermometer probe (FX-9020; Anritsu Meter, Tokyo, Japan). Control cells were not treated with 4-*S*-CAP or hyperthermia.

The antiproliferative effect of the treatment was determined after a 2-day incubation period. The number of viable cells was evaluated by the trypan blue dye-exclusion method using a hemocytometer, and the relative cell number was calculated as follows:

$$\text{Relative cell number (\%)} = (\text{number of viable experimental cells/number of viable control cells}) \times 100.$$

The combined effect of 4-*S*-CAP and hyperthermia was evaluated using a method reported previously.[18] With [A], [B] and [A + B] representing the percentage cell viability for treatments A and B and the combination treatment A + B, the combined effects were defined as follows: synergistic, $[A + B] < [A] \times [B]/100$; additive, $[A + B] = [A] \times [B]/100$; subadditive, $[A] \times [B]/100 < [A + B] < [A]$, if $[A] < [B]$; interference, $[A] < [A + B] < [B]$, if $[A] < [B]$; and antagonistic, $[B] < [A + B]$, if $[A] < [B]$.

Preparation of 4-*S*-CAP/MCL. Magnetite nanoparticles (Fe_3O_4; average particle size, 10 nm) were the kind gift of Toda Kogyo (Hiroshima, Japan). 4-*S*-CAP was synthesized as described by Padgette *et al.*[19] For the preparation of 4-*S*-CAP/MCL, 0–32 mg of 4-*S*-CAP was added to a lipid mixture consisting of *N*-(α-trimethylammonioacetyl)-didodecyl-D-glutamate chloride (2.78 mg; Sogo Pharmaceutical, Tokyo, Japan), dilauroylphosphatidylcholine (6.64 mg; Sigma Chemical, St Louis, MO, USA) and dioleoylphosphatidyl-ethanolamine (5.58 mg; Sigma Chemical) dissolved in methanol (2 mL), and the mixture was dried down by evaporation for a minimum of 5 h. Then, the lipids containing 4-*S*-CAP were hydrated by vortexing with colloidal magnetite nanoparticles (20 mg/mL, 2 mL) and the liposomes were sonicated for 20 min (28 W). The size of the 4-*S*-CAP/MCL was measured using a dynamic light scattering spectrophotometer (FRAR 1000; Otsuka Electronics, Osaka, Japan).

Antiproliferative activity of 4-*S*-CAP in 4-*S*-CAP/MCL. B16 cells, or NHDF cells as a non-melanocytic control, were plated in six-well cell culture plates at 5×10^4 cells/well with experimental media containing 4-*S*-CAP/MCL at the indicated concentration. The antiproliferative activity was determined after the 2-day incubation period. The number of viable cells was measured by the trypan blue dye-exclusion method using a hemocytometer, and the relative cell number was calculated.

Uptake of 4-*S*-CAP/MCL by B16 cells. B16 cells were cultured to approximately 80% confluence before treatment with 4-*S*-CAP/MCL. Cells were then incubated with experimental media containing 4-*S*-CAP/MCL at a concentration of 43 μg magnetite/mL (4-*S*-CAP, 100 μM), and cells were incubated at 37°C with gentle shaking using a rotary shaker (SHK-320; Asahi Technoglass, Tokyo, Japan). After incubation for 24 h, the cells were washed twice with phosphate-buffered saline and harvested and the magnetite concentration was measured in accordance with our reported method.[7] Briefly, the harvested cells were dissolved completely in 0.2 mL of concentration HCl, after which 1 mL of 5% trichloroacetic acid was added. These mixtures were centrifuged in order to remove aggregates and the supernatants were measured by the potassium thiocyanate method.[20]

***In vitro* magnetite nanoparticle-induced hyperthermia.** An *in vitro* hyperthermia experiment using magnetite nanoparticles was carried out using our previously described method.[7] Briefly, B16 cells were cultured to approximately 80% confluence. Cells were then incubated with experimental media containing 4-*S*-CAP/MCL at a concentration of 43 μg magnetite/mL (4-*S*-CAP, 100 μM). At 24 h after the magnetite incorporation, the cells were collected in a microcentrifuge tube and centrifuged gently in order to form a cell pellet. The tube was then placed at the center of the coil of a high-frequency magnetic field generator (360 kHz, 120 Oe; Daiichi High Frequency, Tokyo, Japan). The temperature of the cell pellet was measured by inserting an optical fiber probe into its center, and the pellet was maintained at a constant temperature by manually tuning the strength of the magnetic field. The duration of the AMF irradiation was 30 min. During AMF irradiation, the temperature of the environment was maintained at 37°C. The treated cells were reseeded in a six-well cell culture plate at 2×10^4 cells/well. The number of viable cells was measured by the trypan blue exclusion method using a hemocytometer.

***In vivo* magnetite nanoparticle-induced hyperthermia.** When melanoma nodules grew to 5 mm in diameter, the tumor-bearing mice were separated into five groups (day 0). Mice in group I (control) were the non-treated control. Mice in groups II (MCL) and IV (MCL + AMF) received intratumoral injection of MCL (0.2 mL, 20 mg magnetite/mL). Mice in groups III (4-*S*-CAP/MCL) and V (4-*S*-CAP/MCL + AMF) received intratumoral injection of 4-*S*-CAP/MCL (0.2 mL; 20 mg/mL magnetite; 100 μM 4-*S*-CAP). At 1 day after the injection of MCL or 4-*S*-CAP/MCL (day 1), mice in groups IV (MCL + AMF) and V (4-*S*-CAP/MCL + AMF) were subjected to AMF for 30 min in a coil with a transistor inverter. Magnetic field frequency and intensity were 118 kHz and 384 Oe, respectively. Tumor and rectal temperatures were measured using an optical fiber probe. Subsequently, after the AMF irradiation, MCL or 4-*S*-CAP/MCL were again injected into the mice in groups II and IV or groups III and V, respectively. At 1 day after the second injection (day 2), mice in groups IV (MCL + AMF) and V (4-*S*-CAP/MCL + AMF) were again subjected to AMF for 30 min. During the injection of MCL or 4-*S*-CAP/MCL and AMF irradiation, tumor-bearing mice were anesthetized with pentobarbital sodium (50 mg/kg intraperitoneally).

For histological examination, the tumor was resected and fixed in a 10% formalin solution 24 h after hyperthermia. The specimens were fixed in 10% neutrally buffered formalin, and embedded in paraffin. Serial specimens were then prepared for histological examination, and were stained with hematoxylin and eosin (H&E).

Statistical analysis. Statistical analysis was carried out by the Mann–Whitney rank sum test calculated using WinSTAT statistical software (Light Stone International, Tokyo, Japan). Differences were considered to be statistically significant at $P < 0.05$.

Results

Combined effect of 4-*S*-CAP and hyperthermic treatment. Figure 1 shows the relative cell number for B16 cells on the second day

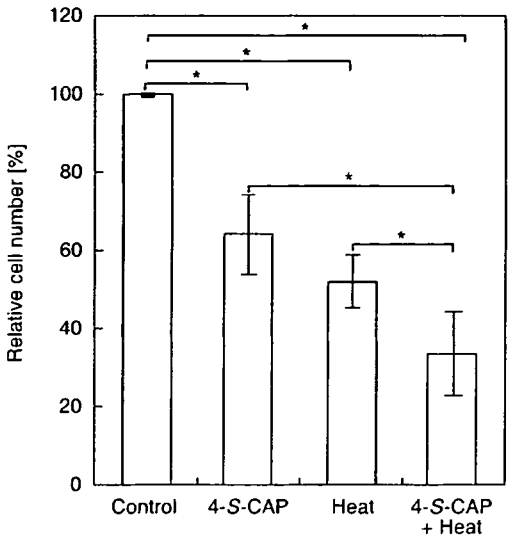

Fig. 1. Combined effects of 4-*S*-cysteaminylphenol (4-*S*-CAP) and heat treatment on B16 cell viability. B16 cells were treated with 4-*S*-CAP at 50 μM. Simultaneously, the cells were heated using a water bath at 42.5°C for 1 h. After the 2-day incubation period, antiproliferative effects were assessed as the relative cell number (%). Data and bars are mean ± SD of two independent experiments. $*P < 0.05$.

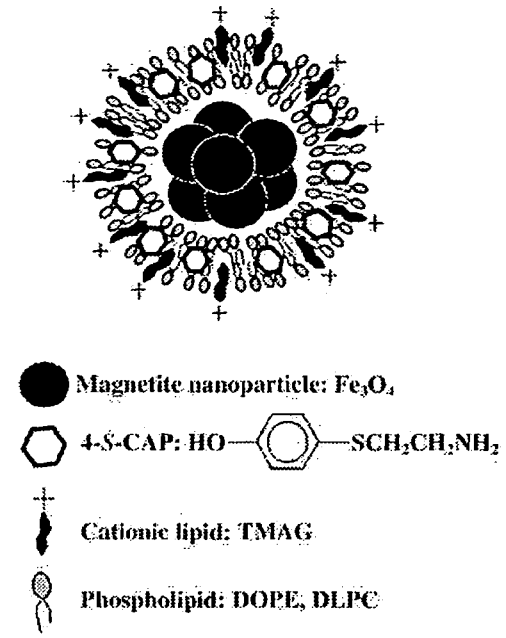

Fig. 2. Preparation of 4-*S*-cysteaminylphenol (4-*S*-CAP)/magnetite cationic liposomes (MCL). Illustration of 4-*S*-CAP/MCL is shown.

after hyperthermic treatment using a 42.5°C water bath for 60 min. For hyperthermic treatment alone, the relative cell number was 52.5 ± 6.6%. For 4-*S*-CAP (50 μM) treatment alone, the relative cell number was 64.4 ± 9.9%. When hyperthermic treatment was combined with 4-*S*-CAP treatment, the relative cell number decreased to 33.7 ± 10.6%. With [A], [B] and [A + B] representing the percentage cell viability for treatments of 4-*S*-CAP, heat and the combination treatment 4-*S*-CAP + heat, respectively, the combined effects were defined as follows: synergistic, [A + B] < [A] × [B]/100; additive, [A + B] = [A] × [B]/100; subadditive, [A] × [B]/100 < [A + B] < [A], if [A] < [B]; interference, [A] < [A + B] < [B], if [A] < [B]; and antagonistic, [B] < [A + B], if [A] < [B]. Here, [A + B] and [A] × [B]/100 were 33.7 ± 10.6% and 34.1 ± 9.5%, respectively. Because there was no significant difference ($P = 0.56$) between [A + B] and [A] × [B]/100, the combined effect of 4-*S*-CAP with heat was evaluated as additive effects.

Preparation of 4-*S*-CAP-loaded MCL. Because the combination of 4-*S*-CAP and hyperthermia has an additive effect, we constructed 4-*S*-CAP/MCL (Fig. 2) and investigated whether 4-*S*-CAP/MCL can combine 4-*S*-CAP-mediated chemotherapy with MCL-induced hyperthermia. The size distribution of 4-*S*-CAP/MCL with various 4-*S*-CAP contents was measured using a dynamic light-scattering spectrophotometer (Fig. 3). For MCL without 4-*S*-CAP, the peak in the particle size distribution was 124.5 ± 0.95 nm (the mean ± SD of three independent experiments). The average size of 4-*S*-CAP/MCL increased drastically when the 4-*S*-CAP concentration exceeded 100 μM. When the 4-*S*-CAP concentration exceeded 100 μM, the dispersibility of 4-*S*-CAP/MCL was extremely low and precipitation of 4-*S*-CAP/MCL was observed. Therefore, 4-*S*-CAP/MCL at 100 μM of 4-*S*-CAP concentration was used in the following *in vivo* experiments.

Antiproliferative activity of 4-*S*-CAP in 4-*S*-CAP/MCL. Figure 4a shows the antiproliferative effects of different concentrations of 4-*S*-CAP/MCL on B16 cells. The dose–response curve showed a dose-dependent antiproliferative effect for 4-*S*-CAP in 4-*S*-CAP/MCL, with the maximum effects achieved using a concentration of 400 μM (46.6 ± 0.9% of relative cell number), which was comparable to the cytotoxicity of free 4-*S*-CAP (inhibition

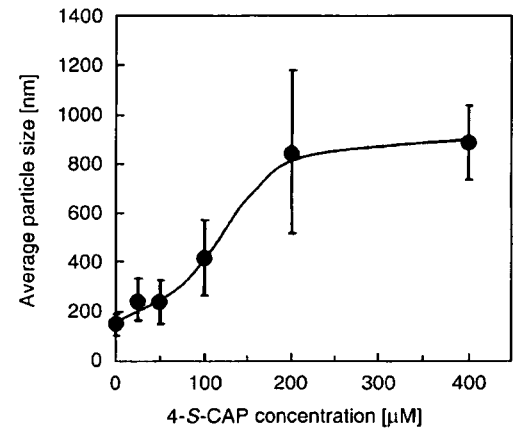

Fig. 3. Relationship between 4-*S*-cysteaminylphenol (4-*S*-CAP) concentration and liposome size of 4-*S*-CAP/magnetite cationic liposomes (MCL). The size of the 4-*S*-CAP/MCL was measured using a dynamic light scattering spectrophotometer. Data and bars are mean ± SD of three independent experiments.

concentration [IC_{50}] IC_{50} of 507 μM) toward B16 melanoma cells.[21] Figure 4b shows the time course of the relative cell number when B16 or NHDF cells were treated with 100 μM 4-*S*-CAP/MCL. The relative cell number for B16 cells decreased linearly to 60% during the 2-day culture period. In contrast, non-melanocytic NHDF cells showed no decrease in relative cell number 1 day after 4-*S*-CAP/MCL treatment, with only slight antiproliferative effects (15% decrease in the relative cell number) observed on day 2. These results indicate that 4-*S*-CAP in 4-*S*-CAP/MCL had an antiproliferative effect on B16 cells, although 4-*S*-CAP was less toxic to non-melanocytic NHDF cells, an observation that corresponds to previous reports.[22]

Uptake of magnetite nanoparticles by B16 cells and *in vitro* hyperthermia. Next, in order to assess the feasibility of magnetite nanoparticle-mediated hyperthermia *in vitro*, we investigated whether 4-*S*-CAP/MCL

doi: 10.1111/j.1349-7006.2006.00382.x

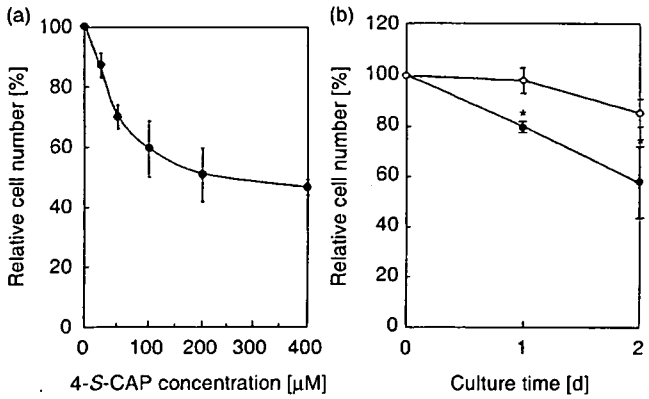

Fig. 4. Antiproliferative activity of 4-*S*-cysteaminylphenol (4-*S*-CAP) mediated by 4-*S*-CAP/magnetite cationic liposomes (MCL). (a) B16 cells were treated with different concentrations of 4-*S*-CAP/MCL (4-*S*-CAP, 0–400 μM). After the 2-day incubation period, antiproliferative effects were assessed as the relative cell number (%). Data and bars are mean ± SD of three independent experiments. (b) B16 (●) and normal human dermal fibroblasts (NHDF) (○) cells were treated with 4-*S*-CAP/MCL at 100 μM 4-*S*-CAP, and the relative cell number was assessed on days 1 and 2. Data and bars are mean ± SD of three independent experiments. $*P < 0.05$.

were incorporated into B16 cells. The uptake of magnetite nanoparticles by B16 cells is shown in Fig. 5a. Magnetite nanoparticles in 4-*S*-CAP/MCL were incorporated into B16 cells, and the amount of uptake was 18.4 ± 1.0 pg magnetite/cell after 24 h, which was comparable to that of MCL (15.0 ± 0.4 pg magnetite/cell).

We then investigated whether AMF irradiation generated heat in B16 cells treated with 4-*S*-CAP/MCL, and observed intracellular hyperthermia *in vitro*. Figure 5b shows the temperature profile of cell pellets treated with 4-*S*-CAP/MCL during AMF irradiation at 360 kHz and 120 Oe. Heat was generated in B16 cells incorporating magnetite nanoparticles. The temperature of these cells rose quickly and reached 43.0°C, which is an effective temperature for hyperthermia treatment, and was then maintained at that temperature for 30 min by controlling the intensity of the AMF. In contrast, in non-treated cells (0 pg magnetite/cell), the temperature increased only 2°C during the AMF irradiation. Figure 5c shows the viable cell number after the AMF irradiation. When the cells were treated with 4-*S*-CAP/MCL alone (without irradiation; 4-*S*-CAP/MCL, 100 μM), the viable cell number decreased to approximately half of that for non-treated cells. Moreover, when the cells were treated with 4-*S*-CAP/MCL plus AMF irradiation, the viable cell number decreased drastically for 1 day and thereafter cells grew again, resulting in an apparently smaller number than with 4-*S*-CAP/MCL alone (without irradiation).

***In vivo* hyperthermic treatment using 4-*S*-CAP/MCL.** For hyperthemic treatment *in vivo*, 4-*S*-CAP/MCL was injected into the tumor and AMF was applied to the whole body of the mouse. Figure 6a shows the tumor surface and rectal temperatures during AMF irradiation. Tumor temperature increased rapidly to 45°C within 3 min and was then maintained for 30 min by controlling the AMF intensity. In contrast, the temperature in the rectum showed only a limited increase during irradiation. These temperature profiles for 4-*S*-CAP/MCL-induced hyperthermia were comparable to those of MCL-induced hyperthermia (data not shown). No serious burns or damage were observed in all mice treated with magnetite-mediated hyperthermia.

For B16 melanoma, the therapeutic effects of the 4-*S*-CAP/MCL-induced combination of chemotherapy and hyperthermia

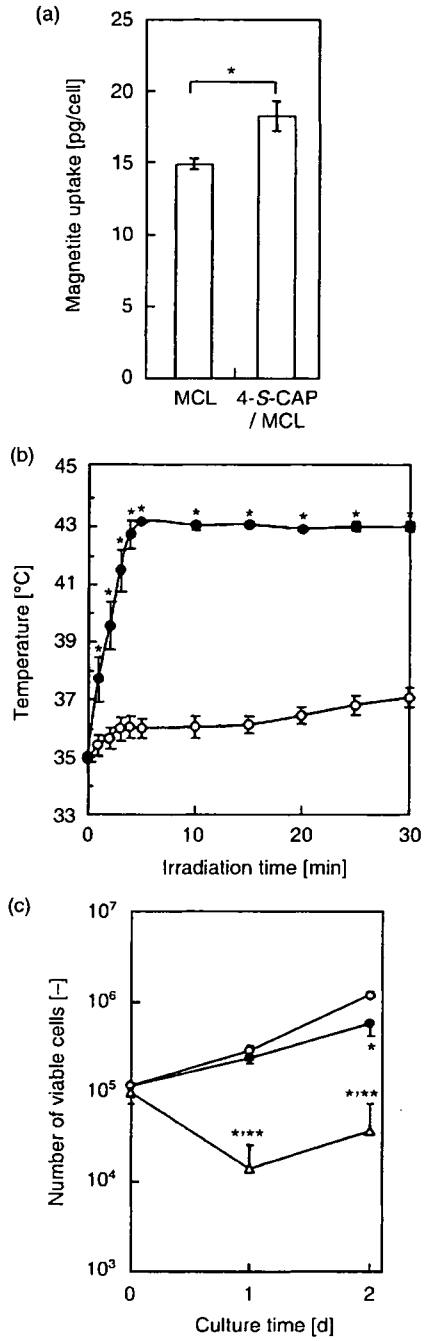

Fig. 5. *In vitro* hyperthermia induced by 4-*S*-cysteaminylphenol (4-*S*-CAP)/magnetite cationic liposomes (MCL). (a) Uptake of magnetite nanoparticles into B16 cells at 24 h after addition of MCL or 4-*S*-CAP/MCL. Percentage magnetite uptake was evaluated. Data and bars are mean ± SD of three independent experiments ($*P < 0.05$). (b) Temperature increase in cell pellets treated with 4-*S*-CAP/MCL during alternating magnetic field (AMF) irradiation. B16 cells with (●) or without (○) 4-*S*-CAP/MCL were irradiated with AMF for 30 min. Data and bars are mean ± SD of three independent experiments ($*P < 0.05$). (c) *In vitro* antiproliferation effects of 4-*S*-CAP/MCL after AMF irradiation. After the AMF irradiation, cells were reseeded and the number of viable cells was measured on the indicated day by the trypan blue exclusion method using a hemocytometer. (○) Control B16 cells; (●) B16 cells with 4-*S*-CAP/MCL; and (△) B16 cells treated with 4-*S*-CAP/MCL and AMF irradiation. Data and bars are mean ± SD of three independent experiments. $*P < 0.05$, significantly different from control group (non-treated B16 cells); $**P < 0.05$, significantly different from 4-*S*-CAP/MCL group (4-*S*-CAP/MCL alone).

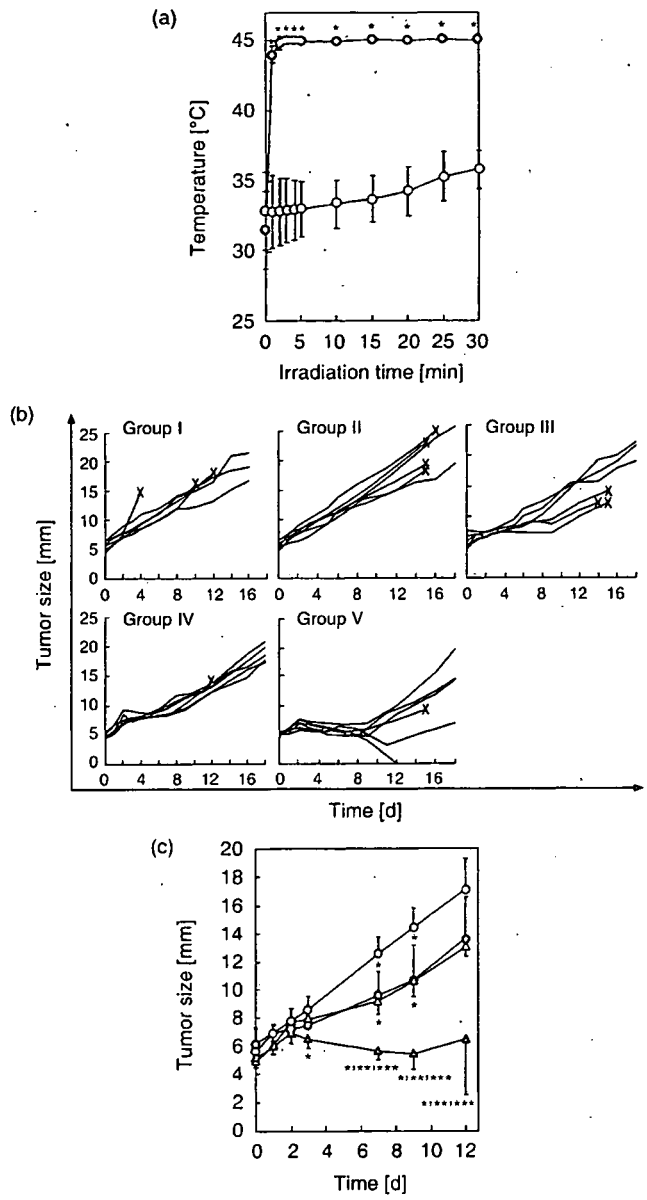

Fig. 6. *In vivo* hyperthermia using 4-*S*-cysteaminylphenol (4-*S*-CAP)/magnetite cationic liposomes (MCL). Schema of the therapeutic experiment. (a) Temperature increase in melanoma nodules treated with 4-*S*-CAP/MCL during alternating magnetic field (AMF) irradiation. 4-*S*-CAP/MCL containing 4 mg magnetite were injected directly into subcutaneous B16 tumors with diameters of 5 mm, which were then irradiated with an AMF for 30 min. Tumor and rectal temperatures were measured using optical fiber probes. (●) Tumor; (○) rectum. Each point represents the mean ± SD of five mice. $*P < 0.01$. (b) Therapeutic effects of 4-*S*-CAP/MCL on B16 tumors. Each line represents tumor growth in a single mouse ($n = 6$). Crosses (×) indicate when each mouse died. (c) Comparison of each group in the first 12 days after treatment. (○) Group II; (●) group III; (△) group IV; (▲) group V. Each point represents the mean ± SD of six mice. $*P < 0.05$, significantly different from group II (MCL alone); $**P < 0.05$, significantly different from group III (4-*S*-CAP/MCL alone); $***P < 0.05$, significantly different from group IV (MCL + AMF).

were assessed. Figure 6b shows the time course of tumor growth in each mouse, and the comparison of tumor growth kinetics in each group in the first 12 days is shown in Fig. 6c. In groups I (control) and II (MCL), tumors grew progressively and some mice died from pulmonary metastases (data not shown). In

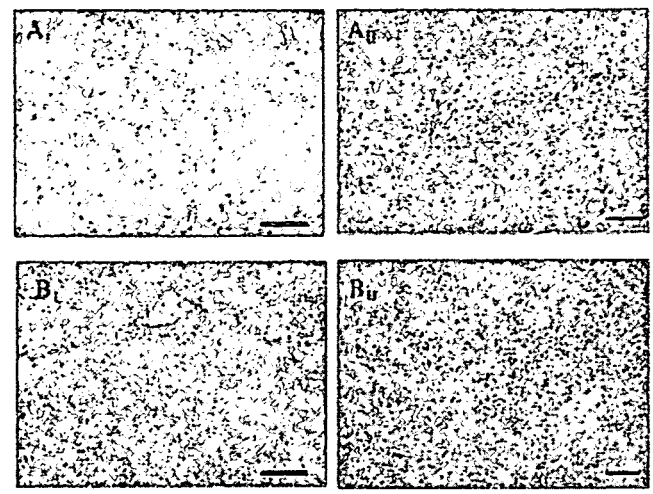

Fig. 7. Pathological features of the tumor in representative mice treated with hyperthermia using 4-*S*-cysteaminylphenol (4-*S*-CAP)/magnetite cationic liposomes (MCL). Tumors of mice in the control group (groups I, A-I and A-II) and 4-*S*-CAP/MCL-induced hyperthermia treatment group (groups IV, B-I and B-II) were stained with hematoxylin and eosin. Scale bars in I and II are 200 μm and 50 μm, respectively.

groups III (4-*S*-CAP/MCL), in which mice received 4-*S*-CAP/MCL alone (without AMF irradiation), and IV (MCL + AMF), in which mice received MCL-induced hyperthermia, tumor growth was slightly but significantly suppressed on days 7 and 9, and thereafter tumors grew progressively. In contrast, in group V (4-*S*-CAP/MCL + AMF), in which mice received 4-*S*-CAP/MCL and AMF irradiation, tumor growth was strongly suppressed in the first 12 days (Fig. 6c), and 17% (1/6) of subcutaneous tumors regressed completely (Fig. 6b). Histological examination of the tumors was done by H&E staining (Fig. 7). Severe necrosis with hemorrhage was observed, and many dead cells with condensed nuclei were seen, as shown in Fig. 7.

Discussion

In the present study, we examined the combination effect of 4-*S*-CAP treatment and hyperthermia on B16 melanoma cells, and demonstrated that the combination therapy has an additive effect (Fig. 1). In normal melanocytes and malignant melanoma cells, the specific enzyme tyrosinase catalyzes the oxidative conversion of L-tyrosine to melanin pigments.[23] 4-*S*-CAP is a good substrate for tyrosinase, and an oxidized form binds to sulphydryl enzymes.[24] With respect to the mechanism of cytotoxicity, dihydro-1,4-benzothiazine-6,7-dione, a metabolite of 4-*S*-CAP, deprives melanoma cells of reduced glutathione and may inactivate SH enzymes essential for DNA synthesis and cell proliferation by covalent binding through their cysteine residues, thereby exerting melanocytotoxicity.[21] Thus, cytotoxicity of 4-*S*-CAP depends mostly on reactive oxygen species (ROS). Similarly to 4-*S*-CAP activities in melanoma cells, hyperthermia can promote the formation of free radicals and related ROS from metabolic pathways, and these ROS may result in some cellular injury.[25] We speculate that ROS played an important role in the additive effect of the combined 4-*S*-CAP treatment and hyperthermia on melanoma cells; therefore, further research is required in order to elucidate the mechanism.

In the case of a superficial tumor, such as melanoma, a simple heat mediator is desirable for the clinical application of hyperthermia. Previously, we confirmed hyperthermic effects on B16

doi: 10.1111/j.1349-7006.2006.00382.x

melanoma using MCL injected directly into the tumor.[26] MCL uptake by cells in the injection site was much higher than that of magnetoliposomes whose liposomal surface had neutral charge, because MCL can electrostatically interact with the negative-charged phospholipid membrane of cells,[7] resulting in retention at the injection site. Thus, in a drug-targeting modality for melanoma, the use of 4-*S*-CAP/MCL is appropriate because superficial tumors can be treated with intratumoral injection of 4-*S*-CAP/MCL. Therefore, we used 4-*S*-CAP/MCL in order to heat the tumoral region and minimize heating of the surrounding healthy tissue. As shown in Fig. 6a, during hyperthermia using 4-*S*-CAP/MCL, tumor temperature reached 45°C rapidly, whereas rectal temperature remained at 38°C. These results indicate that using 4-*S*-CAP/MCL allows the application of hyperthermia to specific tumor tissue and that accurate control of the tumor temperature is possible by manipulating the magnetic field intensity. In this study, we set the tumor temperature at 45°C; however, this was insufficient to completely destroy the malignant melanoma. Our hyperthermia system can be carried out at higher temperatures and can be conducted repeatedly without damaging healthy tissue. For example, complete regression of B16 melanoma was observed in 90% of mice using MCL-induced hyperthermia at 46°C applied once daily for 2 days.[26] In the present study, we set the temperature at 45°C in order to examine the effects of combining hyperthermia with 4-*S*-CAP-madiated chemotherapy.

A major advantage of hyperthermia is that it has few side effects. In contrast to chemotherapy, hyperthermic effects are independent of cell lines and animals.[9–13] Furthermore, hyperthermic effects on cancer cells are caused mainly by physical damage, and differences in sensitivities to hyperthermia are negligible, especially at higher temperatures.[27,28] Therefore, when magnetite nanoparticles are internalized into tumor cells, the hyperthermic effect should be independent of cell type. However, in the case of repeated injection of 4-*S*-CAP/MCL, the toxicity of 4-*S*-CAP/MCL may become an important issue in a clinical trial. For MCL, in our preliminary study, the toxicity of a single administration of MCL solution (33 mg magnetite, intraperitoneally) was investigated. MCL accumulated mostly in the liver and spleen of mice, but none of the five observed mice died after MCL injection.[29] In the present study, 8 mg magnetite was used, which was much less than that used in the preliminary examination (33 mg). The 4-*S*-CAP was synthesized as an antimelanoma agent that is selectively toxic to the *in vivo* melanocytes engaged in melanin synthesis,[30,31] but not to the melanocytes and keratinocytes of albino mice.[31] However, a study by Padgette *et al.* has shown that 4-*S*-CAP is a good substrate of plasma monoamine oxidase, as well as tyrosinase.[19] The cytotoxicity of 4-*S*-CAP to cultured cells may be partly mediated by the aldehyde formed by oxidative deamination.[32] In the present study, non-melanocytic NHDF cells showed a slight decrease in relative cell number (decrease of 15%; Fig. 4b), suggesting that 4-*S*-CAP induced tyrosinase-independent toxicity. However, the mechanism of this tyrosinase-independent toxicity remains to be clarified. Taken together, these findings indicate that 4-*S*-CAP/MCL toxicity should be fully investigated before clinical application.

In conclusion, the promising results of the present study warrant further investigation of new modalities using 4-*S*-CAP/MCL, with the long-term goal of future application in the treatment of malignant melanoma in humans.

Acknowledgments

The authors would like to thank Toda Kogyo Co. for supplying the magnetite. This work was partially supported by a Health and Labour Sciences Research Grant-in-Aid for Research on Advanced Medical Technology from the Ministry of Health, Labour and Welfare, a Grant-in-Aid for University Start-Up Creation Support System, and a 21st Century COE Program 'Nature-Guided Materials Processing' grant from the Ministry of Education, Culture, Sports, Science, and Technology of Japan.

References

1 Van der Zee J. Heating the patient: a promising approach? *Annu Oncol* 2002; **13**: 1173–84.
2 Abe M, Hiraoka M, Takahashi M *et al.* Multi-institutional studies on hyperthermia using an 8-MHz radiofrequency capacitive heating device (Thermotron RF-8) in combination with radiation for cancer therapy. *Cancer* 1986; **58**: 1589–95.
3 Moroz P, Jones SK, Gray BN. Magnetically mediated hyperthermia: current status and future directions. *Int J Hyperthermia* 2002; **18**: 267–84.
4 Jordan A, Wust P, Fahling H, John W, Hinz A, Felix R. Inductive heating of ferrimagnetic particles and magnetic fluids: physical evaluation of their potential for hyperthermia. *Int J Hyperthermia* 1993; **9**: 51–68.
5 Minamimura T, Sato H, Kasaoka S *et al.* Tumor regression by inductive hyperthermia combined with hepatic embolization using dextran magnetite-incorporated microspheres in rats. *Int J Oncol* 2000; **16**: 1153–8.
6 Shinkai M, Matsui M, Kobayashi T. Heat properties of magnetoliposomes for local hyperthermia. *Jpn J Hyperthermic Oncol* 1994; **10**: 168–77.
7 Shinkai M, Yanase M, Honda H, Wakabayashi T, Yoshida J, Kobayashi T. Intracellular hyperthermia for cancer using magnetite cationic liposomes: *in vitro* study. *Jpn J Cancer Res* 1996; **87**: 1179–83.
8 Yanase M, Shinkai M, Honda H, Wakabayashi T, Yoshida J, Kobayashi T. Intracellular hyperthermia for cancer using magnetite cationic liposomes: *ex vivo* study. *Jpn J Cancer Res* 1997; **88**: 630–2.
9 Yanase M, Shinkai M, Honda H, Wakabayashi T, Yoshida J, Kobayashi T. Intracellular hyperthermia for cancer using magnetite cationic liposomes: an *in vivo* study. *Jpn J Cancer Res* 1998; **89**: 463–9.
10 Matsuoka F, Shinkai M, Honda H, Kubo T, Sugita T, Kobayashi T. Hyperthermia using magnetite cationic liposomes for hamster osteosarcoma. *Biomagn Res Technol* 2004; **25**: 3.
11 Ito A, Tanaka K, Honda H, Abe S, Yamaguchi H, Kobayashi T. Complete regression of mouse mammary carcinoma with a size greater than 15 mm by frequent repeated hyperthermia using magnetite nanoparticles. *J Biosci Bioeng* 2003; **96**: 364–9.
12 Kawai N, Ito A, Nakahara Y *et al.* Anticancer effect of hyperthermia on prostate cancer mediated by magnetite cationic liposomes and immune-response induction in transplanted syngeneic rats. *Prostate* 2005; **64**: 373–81.
13 Matsuno H, Tohnai I, Mitsudo K *et al.* Interstitial hyperthermia using magnetite cationic liposomes to inhibit tumor growth of VX-7 transplanted tumor in rabbit tongue. *Jpn J Hyperthermic Oncol* 2001; **17**: 141–50.
14 Miura S, Ueda T, Jimbow K, Ito S, Fujita K. Synthesis of cysteinylphenol, cysteaminylphenol, and related compounds, and *in vivo* evaluation of antimelanoma effect. *Arch Dermatol Res* 1987; **279**: 219–25.
15 Yamada I, Seki S, Matsubara O, Ito S, Suzuki S, Kasuga T. The cytotoxicity of cysteinylcatechols and related compounds to human melanoma cells *in vitro*. *J Invest Dermatol* 1987; **88**: 538–40.
16 Minamitsuji Y, Toyofuku K, Sugiyama S, Yamada K, Jimbow K. Sulfur containing tyrosine analogs can cause selective melanocytotoxicity involving tyrosinase-mediated apoptosis. *J Invest Dermatol Symp Proc* 1999; **4**: 130–6.
17 Ito A, Shinkai M, Honda H, Wakabayashi T, Yoshida J, Kobayashi T. Augmentation of MHC class I antigen presentation via heat shock protein expression by hyperthermia. *Cancer Immunol Immunother* 2001; **50**: 515–22.
18 Valeriote F, Lin H. Synergistic interaction of anticancer agents: a cellular perspective. *Cancer Chemother Rep* 1975; **59**: 895–900.
19 Padgette SR, Herman HH, Han JH, Pollock SH, May SW. Antihypertensive activities of phenyl aminoethyl sulfides, a class of synthetic substrates for dopamine β-hydroxylase. *J Med Chem* 1984; **27**: 1354–7.
20 Owen CS, Sykes NL. Magnetic labeling and cell sorting. *J Immunol Methods* 1984; **73**: 41–8.
21 Hasegawa K, Ito S, Inoue S, Wakamatsu K, Ozeki H, Ishiguro I. Dihydro-1,4-benzothiazine-6,7-dione, the ultimate toxic metabolite of 4-*S*-cysteaminylphenol and 4-*S*-cysteaminylcatechol. *Biochem Pharmacol* 1997; **53**: 1435–44.
22 Parsons PG, Favier D, McEwan M, Takahashi H, Jimbow K, Ito S. Action of cysteaminylphenols on human melanoma cells *in vivo* and *in vitro*: 4-*S*-cysteaminylphenol binds protein disulphide isomerase. *Melanoma Res* 1991; **1**: 97–104.
23 Prota G. *Melanins and Melanogenesis*. New York: Academic Press, 1992.
24 Ito S, Kato T, Ishikawa K, Kasuga T, Jimbow K. Mechanism of selective toxicity of 4-*S*-cysteinylphenol and 4-*S*-cysteaminylphenol to melanocytes. *Biochem Pharmacol* 1987; **36**: 2007–11.
25 Venkataraman S, Wagner BA, Jiang X *et al.* Overexpression of manganese superoxide dismutase promotes the survival of prostate cancer cells exposed to hyperthermia. *Free Radic Res* 2004; **38**: 1119–32.